UNIVERSIDADE DO VALE DO PARAÍBA
INSTITUTO DE PESQUISA E DESENVOLVIMENTO
PROGRAMA DE PÓS-GRADUAÇÃO EM ENGENHARIA BIOMÉDICA

Erick José Nogueira de Andrade

ANALYSIS OF THE SARS-COV-2 VIRUS SPIKE PROTEIN IN 2D AND 3D NEURONAL MODELS OF ALZHEIMER'S DISEASE ASSOCIATED WITH PHOTOBIOMODULATION TREATMENT

ANÁLISE DA PROTEÍNA SPIKE DO VÍRUS SARS-COV-2 EM MODELOS NEURONAIS 2D E 3D DA DOENÇA DE ALZHEIMER ASSOCIADA AO TRATAMENTO COM FOTOBIOMODULAÇÃO

São José dos Campos, SP
2026

Erick José Nogueira de Andrade

ANALYSIS OF THE SARS-COV-2 VIRUS SPIKE PROTEIN IN 2D AND 3D NEURONAL MODELS OF ALZHEIMER'S DISEASE ASSOCIATED WITH PHOTOBIOMODULATION TREATMENT

Master's Dissertation submitted to the Graduate Program in Biomedical Engineering at the University of Vale do Paraíba, in partial fulfillment of the requirements for the degree of Master of Science in Biomedical Engineering.

Advisor: Prof. Dr. Cristina Pacheco-Soares

São José dos Campos, SP
2026

Fundação Valeparaibana de Ensino

BIBLIOTECA

TERMO DE AUTORIZAÇÃO DE DIVULGAÇÃO DA OBRA

Ficha catalográfica

Andrade, Erick José Nogueira de

Análise da proteína Spike do vírus Sars-Cov-2 em modelos neuronais 2D e 3D da doença de Alzheimer associada ao tratamento com fotobiomodulação / Erick José Nogueira de Andrade; orientadora, Cristina Pacheco Soares. - São José dos Campos, SP, 2026.

1 CD-ROM, 65 p.

Dissertação (Mestrado Acadêmico) - Universidade do Vale do Paraíba, São José dos Campos. Programa de Pós-Graduação em Engenharia Biomédica.

Inclui referências

1. Engenharia Biomédica. 2. Alzheimer's Disease. 3. SARS-CoV-2. 4. Spike Protein. 5. Neuroprotection. I. Soares, Cristina Pacheco, orient. II. Universidade do Vale do Paraíba. Programa de Pós-Graduação em Engenharia Biomédica. III. Título.

Eu, Erick José Nogueira de Andrade, autor(a) da obra acima referenciada:

Autorizo a divulgação total ou parcial da obra impressa, digital ou fixada em outro tipo de mídia, bem como, a sua reprodução total ou parcial, devendo o usuário da reprodução atribuir os créditos ao autor da obra, citando a fonte.

Declaro, para todos os fins e efeitos de direito, que o Trabalho foi elaborado respeitando os princípios da moral e da ética e não violou qualquer direito de propriedade intelectual sob pena de responder civil, criminal, ética e profissionalmente por meus atos.

São José dos Campos, 17 de Abril de 2026.

Erick José N. Andrade

Autor(a) da Obra

Data da defesa: 11 / 02 / 2026

UNIVERSIDADE DO VALE DO PARAÍBA

IP&D UNIVAP

ERICK JOSÉ NOGUEIRA DE ANDRADE

"ANÁLISE DA PROTEÍNA SPIKE DO VÍRUS SARS-COV-2 EM MODELOS NEURONAIS 2D E 3D DA DOENÇA DE ALZHEIMER ASSOCIADA AO TRATAMENTO COM FOTOBIOMODULAÇÃO."

Dissertação aprovada como requisito parcial à obtenção do grau de Mestre, do Programa de Pós-Graduação em Engenharia Biomédica, do Instituto de Pesquisa e Desenvolvimento da Universidade do Vale do Paraíba - Univap, pela seguinte banca examinadora:

Prof.ª Dr.ª Cristina Pacheco Soares	Cristina Pacheco Soares
Prof.ª Dr.ª Luciana Barros Sant'Anna	
Prof.ª Dr.ª Cristiane Yumi Koga Ito - Unesp	

Prof.ª Dr.ª Juliana Ferreira Strixino

Diretora do IP&D – Univap

São José dos Campos, 11 de fevereiro de 2026.

DEDICATION

First and foremost, to God. He, who so many times heard me directly and, at other times, through our Holy Mother, was always with me. He listened to my anguish, sadness, and tears, but also to my laughter, joy, and gratitude. In our most sincere and spontaneous conversations, He never allowed me to give up, always strengthening me and showing me how much I could trust.

To my parents, Silvio and Valeria, who never stopped supporting me and wanting to see me happy, no matter what my dream was. You taught me that doing what we love makes us happy and gives us the strength to keep moving forward, because that is what truly matters. Thank you for always prioritizing my education and my opportunities, even in difficult times, because we know that through this path we can change the world and our own reality.

To my goddaughter Clara, who, just like her name, brought light into my life and came into this world while I was in the middle of this work. She showed me and shaped me into a new understanding of love, making me realize that there is a life full of love, happiness, and hope beyond work.

To my professors and mentors. Especially to my advisor, Dr. Cristina, for being so compassionate and an outstanding professor who is always supportive and willing to help, often placing us, her students, above everything else. And to Dr. Geisa, for all the support and guidance, and for being a postdoctoral researcher who always cared about both our knowledge and our humanity, becoming a constant and dear friend.

To my friends, who witnessed and shared my best moments, but who, above all, never abandoned me in the worst ones. You stood by me in times when even I did not believe in myself or in a future. Thank you for not letting go of my hand but instead encouraging me to move forward along a path that was often dark, yet illuminated by the candle you placed in my hands along the way.

And last, but not least, to myself, Erick. Who knows well what he has been through, the struggles he faced, the anxiety he battled. But also the joy this entire journey brought, the friends and colleagues I met, the people who crossed my path, the new places I discovered, and above all, the road I traveled to reach the top of this mountain and be able to say, "I overcame”. Verso I’ alto!

“Do not try to obtain by other means what
you can’t obtain by love.”

St. Francis de Sales

POTENTIAL IMPACT OF THE RESEARCH

The proposed research aims to directly contribute to the Sustainable Development Goals (SDGs), with emphasis on SDG 3 (Good Health and Well-being). The expected impact encompasses different areas: 1) Scientific and Technical Impact: This study advances the understanding of spike protein-induced neurotoxicity in Alzheimer's disease models by employing innovative 2D and 3D approaches. The standardization of 3D spheroids represents a methodological advancement, as it more accurately mimics the complexity of in vivo nervous tissue. Furthermore, the investigation of photobiomodulation (PBM) expands knowledge regarding non-pharmacological therapies for mitochondrial modulation and structural neuronal protection. 2) Social Impact: The research addresses major public health challenges, such as population aging and the increasing prevalence of neurodegenerative diseases. By exploring mechanisms of neuroprotection, it contributes to the development of strategies aimed at delaying disease progression and improving the quality of life of patients and their families. It also reinforces the importance of understanding the neurological sequelae associated with post-COVID syndrome. 3) Innovative and Economic Impact: LED-based PBM stands out as a low-cost, accessible adjuvant therapy with fewer adverse effects compared to conventional pharmacological treatments. The validation of this technology opens perspectives for sustainable healthcare interventions, particularly in resource-limited settings**.** 4) Educational and Cultural Impact: This work promotes high-level academic training through the application of advanced cell culture and microscopy techniques. The findings serve as educational material and as a foundation for outreach activities, strengthening scientific dissemination and professional training in the fields of health sciences and biomedical engineering. 5) Internationalization and Local Integration: Given the global nature of Alzheimer's disease and COVID-19, the results engage with the international scientific literature and foster opportunities for external collaborations. Simultaneously, the research strengthens Brazilian science by generating relevant knowledge within a national institution. 6) Sustainable Development and Related SDGs: The study aligns with SDG 3 (Good Health and Well-being) by promoting quality of life. It also relates to SDG 4 (Quality Education)**,** SDG 9 (Industry, Innovation, and Infrastructure) through the development of accessible technologies, and SDG 10 (Reduced Inequalities) by focusing on low-cost therapeutic strategies.

ABSTRACT

Alzheimer's disease (AD) is the leading cause of dementia worldwide, characterized by a complex pathophysiological scenario involving neuroinflammation and intense oxidative stress. At the same time, the COVID-19 pandemic has raised concerns about the neurodegenerative effects of the SARS-CoV-2 spike protein. Considering that oxidative stress is a central mechanism shared by both AD and the sequelae of COVID-19, this work used hydrogen peroxide (H_2O_2) as an experimental model of oxidative insult. The objective was to investigate how the spike protein enhances cellular damage and to evaluate the neuroprotective potential of photobiomodulation (PBM) with red LED (660 nm) in these contexts. For this, SH-SY5Y cells differentiated into two-dimensional (2D) and three-dimensional (3D) neuronal models were used. The cells were exposed to recombinant spike protein (0.5 µg/mL) and H_2O_2 (200 µM), either individually or in combination, to simulate an aggravated toxicity environment. Cell viability and metabolism were monitored using the Alamar Blue assay and flow cytometry (Live/Dead). Confocal microscopy analyses allowed for the evaluation of nuclear (Hoechst), mitochondrial (MitoTracker), cytoskeletal (rhodamine-phalloidin), and focal adhesion (FAK) integrity. Additionally, a model of neuronal spheroids (3D) was standardized to mimic a more physiologically relevant microenvironment. The results in the 2D model indicated that the spike protein and H_2O_2 significantly reduced cell viability, with intensified cytotoxic effects upon co-exposure. In contrast, the 3D model exhibited an adaptive response, maintaining viability and increasing metabolic activity, suggesting that tissue architecture modulates neuronal resilience. PBM (3 J/cm²) proved effective in preserving mitochondrial and structural morphology, reducing apoptosis both under basal conditions and oxidative stress, especially in the 3D model. Together, the data reinforce that the Spike protein exerts distinct effects depending on the cellular model and highlight PBM as a promising therapeutic strategy to mitigate oxidative stress and preserve neuronal function in neurodegenerative pathologies and viral sequelae.

Keywords: Alzheimer's disease; SARS-CoV-2; spike protein; oxidative stress; photobiomodulation; three-dimensional models; neuroprotection.

RESUMO

A doença de Alzheimer (DA) é a principal causa de demência em todo o mundo, caracterizada por um cenário fisiopatológico complexo envolvendo neuroinflamação e intenso estresse oxidativo. Ao mesmo tempo, a pandemia de COVID-19 levantou preocupações sobre os efeitos neurodegenerativos da proteína spike do SARS-CoV-2. Considerando que o estresse oxidativo é um mecanismo central compartilhado tanto pela Doença de Alzheimer (DA) quanto pelas sequelas da COVID-19, este trabalho utilizou peróxido de hidrogênio (H_2O_2) como um modelo experimental de insulto oxidativo. O objetivo foi investigar como a proteína spike aumenta o dano celular e avaliar o potencial neuroprotetor da fotobiomodulação (PBM) com LED vermelho (660 nm) nesses contextos. Para isso, foram utilizadas células SH-SY5Y diferenciadas em modelos neuronais bidimensionais (2D) e tridimensionais (3D). As células foram expostas à proteína spike recombinante (0,5 μg/mL) e H_2O_2 (200 μM), individualmente ou em combinação, para simular um ambiente de toxicidade agravada. A viabilidade celular e o metabolismo foram monitorados usando o ensaio Alamar Blue e citometria de fluxo (Live/Dead). As análises de microscopia confocal permitiram a avaliação da integridade nuclear (Hoechst), mitocondrial (MitoTracker), do citoesqueleto (rhodamina-faloidina) e das adesões focais (FAK). Além disso, um modelo de esferoides neuronais (3D) foi padronizado para imitar um microambiente mais fisiologicamente relevante. Os resultados no modelo 2D indicaram que a proteína spike e o H_2O_2 reduziram significativamente a viabilidade celular, com efeitos citotóxicos intensificados após a coexposição. Em contraste, o modelo 3D exibiu uma resposta adaptativa, mantendo a viabilidade e aumentando a atividade metabólica, sugerindo que a arquitetura do tecido modula a resiliência neuronal. A PBM (3 J/cm²) provou ser eficaz na preservação da morfologia mitocondrial e estrutural, reduzindo a apoptose tanto em condições basais quanto sob estresse oxidativo, especialmente no modelo 3D. Juntos, os dados reforçam que a proteína Spike exerce efeitos distintos dependendo do modelo celular e destacam a PBM como uma estratégia terapêutica promissora para mitigar o estresse oxidativo e preservar a função neuronal em patologias neurodegenerativas e sequelas virais.

Palavras-chave: doença de Alzheimer; SARS-CoV-2; proteína spike; estresse oxidativo; fotobiomodulação; modelos tridimensionais; neuroproteção.

LIST OF FIGURES

Figure 1 – Pathology of Alzheimer's Disease: Comparison between a healthy brain and a brain with Alzheimer's, highlighting the disintegration of microtubules due to hyperphosphorylation of the TAU protein. 18
Figure 2 – Viral Entry Mechanism of Sars-CoV-2 thru the binding of the Spike protein to the Angiotensin-Converting Enzyme (ACE2). 22
Figure 3 - Stages of SH-SY5Y cell spheroid formation in brightfield. From left to right: monolayer culture (2D Cells); initial sedimentation and aggregation phase in agarose microwells (Seeded Cells); and the finalized three-dimensional model (Spheroids), showing high compactness and homogeneous structural organization after 7 days of cultivation. 33
Figure 4 - Structural analysis by Scanning Electron Microscopy (SEM) of SH-SY5Y neural spheroids. The panels on the left present the organization of the spheroids arranged in agarose microwells, while the panels on the right exhibit the surface morphology at higher magnification. (Control Group): High cellular compaction, architectural integrity, and a regular outer surface are observed, characteristic of stable and cohesive three-dimensional models. (Exposed Group): Exposure to the SARS-CoV-2 spike protein resulted in loss of cellular compactness and irregularity in the outer border of the spheroid, which assumed a rough and heterogeneous appearance, indicating impairment of adhesion and structural organization after the viral challenge. 34
Figure 5 - Cytoviability of 2D neuronal cells model following exposure to Spike protein and/or H_2O_2-induced oxidative stress, with or without PBM. Cell viability is expressed as a percentage relative to the corresponding control group after treatment with H_2O_2 (200 µM), Spike protein (0.5 µg/mL), or their combined exposure (Spike + H_2O_2). Data are presented as mean ± standard deviation. Groups were evaluated 2 h post-irradiation (660 nm, 3 J/cm²). PBM significantly mitigated the cytotoxic effects induced by Spike protein exposure, preserving neuronal viability. Statistical significance compared with the respective control group is denoted by *** ($p < 0.001$), **** ($p < 0.0001$) and ns nonsignificative. 36
Figure 6- Cytoviability of 3D neuronal cells model following exposure to Spike protein and/or H_2O_2-induced oxidative stress, with or without PBM. Cell viability is expressed as a percentage relative to the corresponding control group after treatment with H_2O_2 (200 µM), Spike protein (0.5 µg/mL), or their combined exposure (Spike + H_2O_2). Data are presented as mean ± standard deviation. Groups were evaluated 2 h post-irradiation (660 nm, 3 J/cm²). Spike protein exposure within the 3D microenvironment increased cell viability. Under PBM, no statistical difference was observed between groups. Statistical significance compared with the respective control group is denoted by ** ($p < 0.01$), ns nonsignificative. 37
Figure 7– Viability and apoptosis analysis by flow cytometry in a 3D neuronal model. The populations of live and apoptotic cells were quantified after exposure to H_2O_2 (200 µM) and the Spike protein (0.5 µg/mL), treated or not with PBM (660 nm, 3 J/cm^3). The bars represent the mean ± SD of the cell percentage. It is noted that the spike protein alone induced the highest rate of apoptosis, yet exerted a cytoprotective effect against H_2O_2 in the combined exposure. PBM promoted the maintenance of viability

and reduction of apoptosis in all groups under stress, affirming its neuroprotective potential..... 38
Figure 8 – Micrographs of differentiated neuronal nuclei, non-irradiated (top row) and irradiated with PBM (bottom row) in a 2D model under the following conditions: Control, H_2O_2, Spike, and Spike + H_2O_2 stained with DAPI. Control cells exhibited uniformly distributed nuclei with preserved morphology. H_2O_2 induced chromatin condensation and nuclear fragmentation (red arrow). Cells exposed to the spike protein showed reduced nuclear density and moderate chromatin condensation (yellow arrow). The Spike + H_2O_2 group exhibited severe nuclear damage. The groups treated with PBM exhibited nuclei with less condensation and better structural preservation. Scale bars: 10 µm. 40
Figure 9 - Micrographs of differentiated neuronal nuclei, non-irradiated (top row) and irradiated with PBM (bottom row) in a 3D model under the following conditions: Control, H_2O_2, Spike, and Spike + H_2O_2. In the control group, high cell density with intact nuclei and compact distribution is observed, typical of stable three-dimensional organization. Exposure to H_2O_2 resulted in loss of spheroid compaction and signs of nuclear fragmentation. In the Spike group, a partial maintenance of the architecture is noted, although with slight heterogeneity in nuclear morphology. The Spike + H_2O_2 group exhibited the most severe impairment, with a significant reduction in nuclear density and disintegration of the spheroid structure. The irradiated groups (bottom row) demonstrated partial preservation of structural integrity and a higher density of intact nuclei compared to their respective non-irradiated counterparts, suggesting a protective effect of PBM on the organization of the 3D model. Scale bars: 10 µm. 42
Figure 10 – Micrographs of mitochondrial staining in differentiated neuronal cells, non-irradiated (top row) and irradiated with PBM (bottom row) in a 2D model under the following conditions: Control, H_2O_2, Spike, and Spike + H_2O_2, stained with MitoTracker. Control cells exhibited an organized and reticular mitochondrial appearance. Cells exposed to the spike protein showed reduced intensity and partial fragmentation. Exposure to H_2O_2 induced severe fragmentation (enlarged yellow area) and mitochondrial loss, while the Spike + H_2O_2 group exhibited pronounced perturbations (enlarged white area). The groups treated with PBM demonstrated visibly improved mitochondrial organization and reduced fragmentation. Scale bars: 10 µm 44
Figure 11 - Micrographs of mitochondrial staining in differentiated neuronal cells, non-irradiated (top row) and irradiated with PBM (bottom row) in a 3D model under the following conditions: Control, H_2O_2, Spike, and Spike + H_2O_2. In the control group, an organized and intense mitochondrial network is observed, with a reticular distribution characteristic of viable models. In the group exposed only to the spike protein, a slight reduction in signal intensity and early signs of network fragmentation are noted. Exposure to peroxide resulted in severe impairment, evidenced by a punctate mitochondrial pattern and loss of the network's structural integrity. The Spike + H_2O_2 group presented the most critical state of disorganization, with dispersed fluorescent signal and fragmentation, indicating severe bioenergetic failure. In contrast, the irradiated groups (bottom row) demonstrated mitochondrial organization with visible improvement and reduced fragmentation compared to their

stressed counterparts, suggesting that PBM assisted in preserving mitochondrial function and attenuating the damage induced by the insults. Scale bars: 10 µm..... 46
Figure 12 – Mitochondrial and nuclear morphology of differentiated neuronal cells exposed to the Spike protein, with or without photobiomodulation (PBM) in a 2D model. Immunofluorescence images of non-irradiated groups (top row) and PBM-irradiated groups (bottom row). Mitochondria were labeled with MitoTracker (red), and nuclei were stained with DAPI (blue). PBM (660 nm, 3 J/cm²) attenuated mitochondrial fragmentation and preserved nuclear morphology in the irradiated Spike group, where mitochondria appear less punctate and nuclei exhibit more uniform chromatin compared to the corresponding non-irradiated Spike panel. Scale bars: 10 µm..... 49
Figure 13 – Mitochondrial and nuclear morphology of differentiated neuronal cells exposed to the Spike protein, with or without photobiomodulation (PBM) in a 3D model. Immunofluorescence images of non-irradiated groups (top row) and PBM-irradiated groups (bottom row). Mitochondria labeled with MitoTracker (red) and nuclei with DAPI (blue). In the control group, high cell density and an organized mitochondrial network are observed. Exposure to H_2O_2 and the Spike protein promoted mitochondrial fragmentation (punctate appearance) and nuclear disorganization, with severe damage in the Spike + H_2O_2 group. PBM (bottom row) visibly attenuated these damages, preserving mitochondrial and nuclear morphology, especially in the Spike group, where more uniform chromatin and integrated mitochondria are observed. Scale bars: 10 µm. 50
Figure 14 - Evaluation of nuclear and mitochondrial morphology in a 2D model under oxidative stress, using cells differentiated into a neuronal phenotype under non-irradiated (top row) and PBM-irradiated (660 nm, 3 J/cm²; bottom row) conditions. Nuclei were stained with DAPI (blue) and mitochondria with MitoTracker Orange (red). In the control group, preserved cell confluence and a reticular mitochondrial network are observed. Exposure to H_2O_2 resulted in intense neurite retraction, nuclear condensation, and fragmentation of the mitochondrial network. The Spike + H_2O_2 group exhibited the highest degree of structural damage, with a drastic reduction in cell density. In the irradiated groups (bottom row), an attenuation of cytoplasmic retraction and better preservation of nuclear and mitochondrial integrity are noted compared to their respective stressed controls. Scale bar: 10 µm. 52
Figure 15 - Evaluation of nuclear and mitochondrial morphology in a 3D model under oxidative stress, using cells differentiated into a neuronal phenotype under non-irradiated (top row) and PBM-irradiated (660 nm, 3 J/cm^2; bottom row) conditions. Nuclei were stained with DAPI (blue) and mitochondria with MitoTracker Orange (red). In the control group, high cellular compaction and a homogeneous mitochondrial signal are observed. Exposure to H_2O_2 alone promoted the destabilization of the spheroid architecture, with loss of cohesion and punctate mitochondrial fragmentation. In the Spike + H_2O_2 group, the most severe impairment of tissue integrity is observed, with clear disintegration of the spheroidal structure. The application of PBM (bottom row) contributed to maintaining the compaction of cellular aggregates and stabilizing mitochondrial morphology against oxidative and viral insults. Scale bar: 10 µm... 53
Figure 16 - Cytoskeleton organization, focal adhesion, and nuclear morphology of differentiated neuronal cells exposed or not to the Spike protein in a 2D model. (A) Control condition showing well-organized actin filaments (phalloidin, red), defined focal adhesion sites (FAK, green), and preserved nuclear arrangement (DAPI, blue).

The arrows highlight representative structures: actin filaments (red arrow), focal adhesions (green arrow), and preserved nuclear morphology (blue arrow). (B) Cells exposed to the Spike protein (0.5 µg/mL) exhibited cytoskeleton disorganization, altered FAK distribution, and nuclear condensation. Arrows indicate disorganized actin filaments (red arrow), redistributed focal adhesion points (green arrow), and condensed or irregular nuclei (blue arrow). Scale bars: 20 µm. 55

Figure 17 - Cytoskeleton organization, focal adhesion, and nuclear morphology of differentiated neuronal cells exposed or not to the Spike protein in a 3D model. (A) Control Group: spheroids present an organized architecture, with continuous actin filaments (phalloidin, red), homogeneously distributed FAK labeling (green), and intact nuclei (DAPI, blue), indicating preservation of structural integrity and tissue cohesion. (B) Exposed Group: exposure to the Spike protein (0.5 µg/mL) resulted in significant disorganization of the three-dimensional architecture. Fragmentation of actin filaments, dispersed redistribution of FAK, and nuclei with irregular or condensed morphology are observed, suggesting impairment of adhesion sites and the structural stability of the spheroid. Scale bars: 20 µm. 56

LIST OF TABLES

Table 1- Mechanisms of action and neurotoxic effects of the SARS-CoV-2 S protein in the CNS 15
Table 2 - Reagents, supplements, equipment, and software used in the experimental procedures. 25
Table 3 – Experimental groups and corresponding treatments 29

TABLE OF CONTENTS

1 INTRODUCTION 14
2 OBJECTIVES 16
2.1 GENERAL OBJECTIVE 16
2.2 SPECIFIC OBJECTIVES 16
3 LITERATURE REVIEW 17
3.1 ALZHEIMER'S DISEASE 17
3.2 SH-SY5Y CELL LINE 18
3.3 OXIDATIVE STRESS 19
3.4 RECOMBINANT SPIKE PROTEIN 20
3.5 PHOTOBIOMODULATION 22
3.6 THREE-DIMENSIONAL CELL CULTURE 23
4 METHODOLOGY 25
4.1 STUDY LOCATION 25
4.2 REAGENT AND EQUIPMENT 25
4.2 CELL LINE CULTURE 26
4.2.1 INDUCTION OF OXIDATIVE STRESS 26
4.2.2 EXPOSURE TO THE SPIKE PROTEIN 26
4.3 FABRICATION OF 3D MOLDS 27
4.4 MOLDS MATURATION AND PH EQUILIBRATION 28
4.5 CELL SEEDING AND NEURONAL DIFFERENTIATION 28
4.6 IRRADIATION 29
4.7 CELL VIABILITY 29
4.7.1 ALAMARBLUE ASSAY 29
4.7.2 VIABILITY AND APOPTOSIS ASSESSMENT BY FLOW CYTOMETRY (LIVE/DEAD) 30
4.8 MITOCHONDRIAL AND NUCLEAR ANALYSIS 31
4.9 CELL ADESION AND CYTOSKELETON ANALYSIS 31
4.10 SCANNING ELECTRON MICROSCOPY 32
4.11 STATISTICAL ANALYSIS 32
5 RESULTS AND DISCUSSION 33
5.1 STANDARDIZATION OF THE NEURONAL THREE-DIMENSIONAL MODEL (SH-SY5Y SPHEROIDS) 33
5.2 CELL VIABILITY AND METABOLIC EFFECTS IN NEURONAL MODELS 35
5.2.1 EVALUATION OF METABOLIC VIABILITY BY ALAMAR BLUE 35
5.2.2 CYTO-VIABILITY ANALYSIS BY FLOW CYTOMETRY (LIVE/DEAD) 38

5.3 ALTERAÇÕES NUCLEARES E INTEGRIDADE CELULAR....39
5.4 MITOCHONDRIAL MORPHOLOGY AND FUNCTIONALITY 43
5.5 EFFECTS OF DA PHOTOBIOMODULATION ON VIABILITY AND STRUCTURAL INTEGRITY....48
5.6 OXIDATIVE STRESS AND CELLULAR IMPAIRMENT 51
5.7 CYTOSKELETON ORGANIZATION AND CELL ADHESION 54
6 CONCLUSION 58
REFERENCES 59
ANNEX A – CERTIFICATE OF ANALYSIS OF THE SPIKE PROTEIN 64
ANNEX B – PREPRINT OF THE MANUSCRIPT SUBMITTED TO SPRINGER NATURE 65
ANNEX C – AWARDS AND RECOGNITIONS 66

1 INTRODUCTION

Alzheimer's disease (AD) remains one of the greatest challenges to global public health, being the leading cause of dementia in the elderly (Falco *et al*., 2016). It is a progressive and irreversible neurodegenerative disease, marked by the accumulation of beta-amyloid (Aβ) plaques, hyperphosphorylated Tau protein neurofibrillary tangles, chronic neuroinflammation, and oxidative stress, which culminate in synaptic loss, neuronal death, and severe cognitive decline (Strooper; Karran, 2016). Despite more than a century of research, there are no curative treatments available, and current pharmacological therapies offer only limited symptomatic relief, highlighting the urgency for new therapeutic approaches (Falco *et al*., 2016).

In parallel, the COVID-19 pandemic (Coronavirus Disease), caused by SARS-CoV-2 (Severe Acute Respiratory Syndrome Coronavirus 2), has highlighted concerns about the long-term neurological consequences of the infection (Khan *et al*., 2021). Recent evidence indicates that the spike protein (protein S) of the virus, responsible for cellular invasion via the ACE2 receptor, plays a direct role in neurodegeneration. This mechanism occurs fundamentally because the S1 subunit of the spike protein can cross the blood-brain barrier (Rhea *et al*., 2021) and interact with glial cells, such as astrocytes and microglia (Table 1). This interaction triggers an exacerbated inflammatory response, where the release of pro-inflammatory mediators promotes oxidative stress and mitochondrial dysfunction (Olajide *et al*., 2022). Moreover, the binding of the S protein to the ACE2 receptor reduces the neuroprotective activity of this enzyme, favoring the accumulation of angiotensin II, which has pro-oxidative and pro-degenerative effects (Soheilifar; Fathi; Naghdi, 2021). Studies show that this neurotoxic environment induces hyperphosphorylation of the Tau protein and aggregation of beta-amyloid peptides, mimicking pathologies associated with AD. This neurotoxic potential positions it as an agent of interest for modeling pathogenic mechanisms in in vitro studies (Oh *et al*., 2022).

Table 1 - Mechanisms of action and neurotoxic effects of the SARS-CoV-2 S protein in the CNS

(continue…)

Receptor/Target	Pathogenic Action / Effect	Reference
ACE2	Reduction of neuroprotective activity and increase in Angiotensin II (pro-oxidant).	Soheilifar; Fathi; Naghdi. (2021)

Table 1 - Mechanisms of action and neurotoxic effects of the SARS-CoV-2 S protein in the CNS

(conclusion)

BBB (Blood-Brain Barrier)	Transposition of the S1 subunit into the cerebral parenchyma.	Rhea *et al*. (2021)
Microglia/Astrocytes	Glial activation and release of pro-inflammatory cytokines (Neuroinflammation).	Olajide *et al*. (2022)
Mitochondria	Induction of mitochondrial dysfunction and cellular energy failure.	Oh *et al*. (2022)
Tau Protein / Aβ	Stimulation of Tau hyperphosphorylation and amyloid aggregation.	Oh *et al*. (2022)

Source: Author, 2025.

In this context, photobiomodulation (PBM) emerges as a non-invasive and promising therapeutic modality. Using light in the red spectrum, PBM primarily acts on the mitochondria, promoting an increase in adenosine triphosphate (ATP) production, reduction of oxidative stress, and modulation of the inflammatory response (Hamblin, 2019). Its neuroprotective effects have been demonstrated in preclinical models of neurodegenerative diseases, including the reduction of amyloid plaques and the improvement of cognitive function (Purushothuman *et al*., 2014).

However, most studies in the field still rely on two-dimensional (2D) cell culture models, which, despite their practicality, fail to recapitulate the architectural complexity, cell-cell interactions, and cell-extracellular matrix interactions of neural tissue in vivo (Kapalczynska *et al.*, 2018). Thus, three-dimensional (3D) models, such as spheroids, offer a more physiological environment, allowing the study of nutrient, oxygen, and signaling gradients in a microenvironment that better simulates the human brain (Lancaster; Knoblich, 2014). The adoption of a 3D model is, therefore, relevant for more translational investigations on the pathology of AD and the efficacy of therapeutic interventions.

2 OBJECTIVES

2.1 GENERAL OBJECTIVE

To evaluate the effects of the SARS-CoV-2 S protein in 2D and 3D models of Alzheimer's disease (AD), as well as to investigate the therapeutic potential of red-spectrum LED-based photobiomodulation (PBM) in this context.

2.2 SPECIFIC OBJECTIVES

- Evaluate the effects of the S protein in 2D and 3D cell culture models, analyzing its viability and morphological changes.
- Establish protocols for exposing cell cultures to the S protein, evaluating its effects on cell adhesion, nuclear integrity, and cytoskeletal organization.
- Investigate the therapeutic effects of LED irradiation on cellular parameters affected by the S protein, checking for possible protective or modulatory effects.
- Develop and standardize a 3D cell culture model representative of AD.

3 LITERATURE REVIEW

3.1 ALZHEIMER'S DISEASE

Alzheimer's disease (AD) is the most prevalent neurodegenerative syndrome and the leading cause of dementia worldwide, accounting for approximately 70% of cases. It is characterized by a progressive and irreversible cognitive decline, accompanied by impairments in neurological, cognitive, and behavioral functions, primarily affecting older individuals (Falco *et al.,* 2016).

AD was first described in 1906 by the German neurologist Alois Alzheimer, after observing anatomical and histological alterations in the brain tissue of a patient who presented with mental confusion and behavioral changes. These findings marked the beginning of the clinical and neuropathological characterization of AD (Evangelisti *et al*., 2014).

From a clinical perspective, AD progresses through distinct stages. In the early stage, individuals still retain a certain degree of independence, although they may experience memory lapses, difficulty recalling names and words, or misplacing everyday objects. The intermediate stage is the longest and may last several years, manifesting more pronounced symptoms such as loss of important personal information, language confusion, frustration, and unexpected behaviors, gradually increasing family burden and risk. In the final stage, severe deterioration occurs: patients lose the ability to respond to their environment, exhibit significant motor decline, lose cognitive abilities, and become completely dependent on continuous care (Salameh *et al*., 2015; Fish *et al*., 2019).

The etiological and pathogenic mechanisms of AD have not yet been fully elucidated, although several brain alterations are associated with its development. Among them are the abnormal deposition of beta-amyloid oligomers (AβOs) in the extracellular space, the formation of neurofibrillary tangles resulting from hyperphosphorylation of the Tau protein, neuroinflammation, and atrophy of specific regions such as the hippocampus and cortex (Figure 1). These alterations lead to synaptic loss, neuronal death, and reduced neural connectivity, resulting in brain atrophy, decreased brain volume, and impaired cerebral metabolism (Strooper; Karran, 2016).

Despite more than a century of research, there is no cure for AD, and currently available treatments have limited efficacy. Existing therapies do not halt disease progression but instead aim to control symptoms, with available pharmacological agents contributing primarily to improved quality of life. However, late diagnosis compromises therapeutic response, further

reducing treatment benefits (Falco *et al*., 2016). Moreover, the impact of AD extends beyond the affected individual, representing a major socioeconomic challenge. In 2021, approximately 52.6 million cases of AD and other dementias were estimated worldwide, a number projected to double every two decades, particularly in low- and middle-income countries due to population aging (Zhang; Chai; Wang, 2025).

For this reason, AD remains one of the greatest challenges in modern neuroscience. A deeper understanding of it s molecular and cellular mechanisms is essential for advancing early diagnosis, developing preventive strategies, and establishing more effective therapeutic approaches.

Figure 1 – Pathology of Alzheimer's Disease: Comparison between a healthy brain and a brain with Alzheimer's, highlighting the disintegration of microtubules due to hyperphosphorylation of the TAU protein.

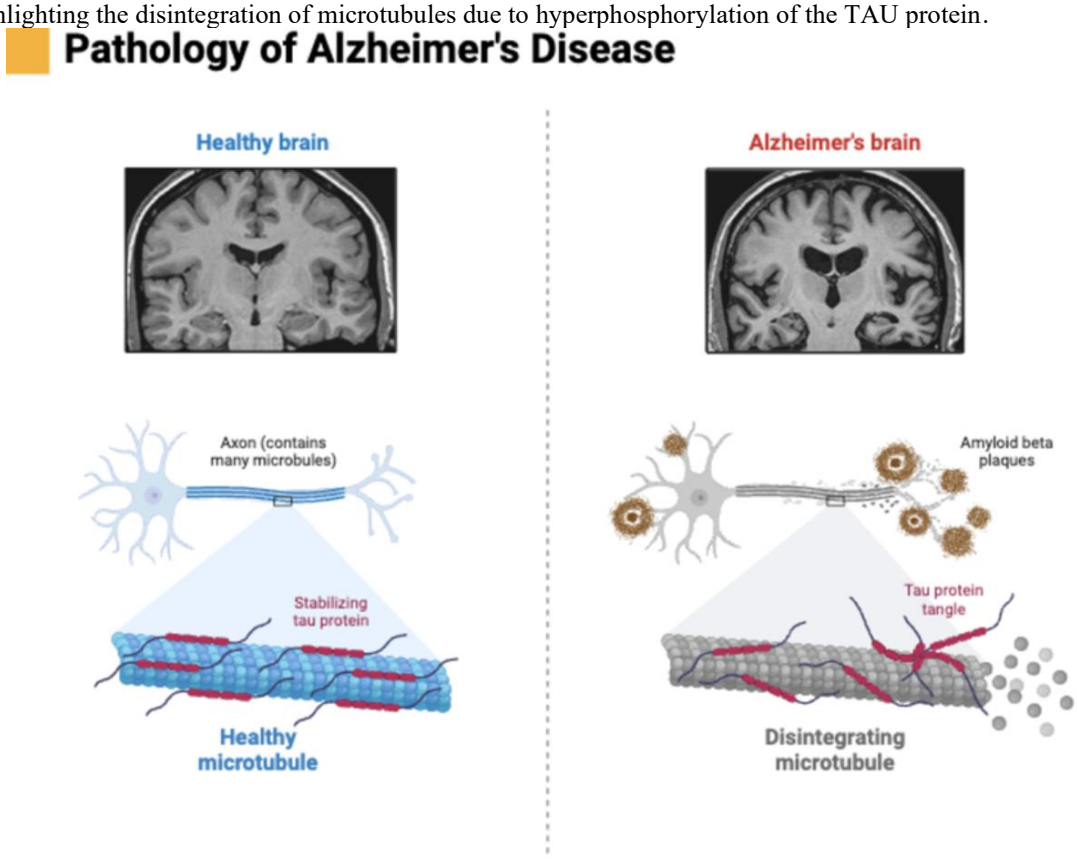

Source: Biorender, 2025.

3.2 SH-SY5Y CELL LINE

The SH-SY5Y cell line is a sublineage cloned three times from the human neuroblastoma line SK-N-SH, established in 1970 from a biopsy of bone metastasis from a four-year-old patient (Biedler *et al*., 1978). This lineage has been widely used as an in vitro

model in neuroscience, immunology, and toxicology research, due to its neuronal characteristics and ease of cultivation (Xicoy; Wrike; Schneider, 2017; Salles, *et al*., 2025).

This lineage exhibits catecholaminergic properties, expressing enzymes such as dopamine beta-hydroxylase, which gives them the ability to synthesize neurotransmitters like dopamine and norepinephrine (Biedler *et al*., 1978). Due to these characteristics, they are frequently used as a model for the study of neurodegenerative diseases, such as Parkinson's disease and AD (Xicoy; Wrike; Schneider, 2017).

Moreover, these cells can be differentiated into mature neuron-like cells thru treatments with retinoic acid, resulting in more pronounced neuronal morphology and increased expression of neuronal markers (Xicoy; Wrike; Schneider, 2017). This differentiation capacity makes it a versatile model for studies investigating neurogenesis and neurotoxicity mechanisms.

In the context of toxicology research, this lineage has been employed to evaluate the neurotoxic effects of various compounds, including pesticides, dioxins, flame retardants, among others. The effects observed in these cells include increased oxidative stress, mitochondrial dysfunction, alterations in neurotransmitter homeostasis, and cell death by apoptosis or necrosis (Feles *et al*., 2022).

In terms of culture, SH-SY5Y cells can grow both in suspension and adhered to the substrate, forming aggregates during cell division that differ significantly from the morphology of cells differentiated into a neuronal model (Feles *et al*., 2022).

In summary, this cell line represents a valuable and well-established tool in the scientific community for studies related to neuronal functions, differentiation mechanisms, and neurotoxicity assessment, significantly contributing to the advancement of knowledge in neuroscience and related fields.

3.3 OXIDATIVE STRESS

Oxidative stress is a physiological imbalance, characterized by the overproduction of reactive oxygen species (ROS) that exceeds the antioxidant defense capacity of cells, resulting in macromolecular damage (Sies; Jones, 2020). Under normal conditions, these species, such as superoxide anion, hydrogen peroxide (H_2O_2), and hydroxyl radical, act as important signaling molecules. However, their excessive production leads to the oxidation of lipids, proteins, and DNA, compromising cellular homeostasis and culminating in cell death (Lushchak, 2014).

As previously described, AD is classically characterized by the deposition of Aβ plaques and neurofibrillary tangles of hyperphosphorylated Tau protein. A robust consensus in the

literature indicates that oxidative stress is not merely an epiphenomenon but a central and early pathogenic mechanism in the disease (Butterfield; Halliwell, 2019). Oxidative stress and Aβ pathology form a vicious cycle. On one hand, Aβ aggregates can induce the production of ROS directly or through the activation of microglia, promoting neuroinflammation (Zhao; Zhao, 2013). On the other hand, oxidative stress favors the cleavage of Amyloid Precursor Protein (APP) via the amyloidogenic pathway, increasing the production of Aβ, which in turn generates more ROS (Cheignon *et al*., 2018).

Neurons are particularly vulnerable to oxidative damage due to their high oxygen consumption, abundance of polyunsaturated fatty acids (targets of lipoperoxidation), and relatively low antioxidant capacity. Oxidative stress in AD is closely linked to mitochondrial dysfunction, where the mitochondrion, which is a primary source of ROS, is also one of its main victims. The failure in the electron transport chain amplifies the production of these species, creating a cycle of bioenergetic decline (Swerdlow, 2018).

To study the mechanisms of AD and test therapeutic interventions such as PBM, the induction of oxidative stress in vitro is a widely validated strategy. Pro-oxidant agents such as H_2O_2 are frequently used to mimic the oxidative environment found in the brains of individuals with AD (Finaud; Lac; Filaire, 2006). This model allows for the investigation of study markers for the disease.

3.4 RECOMBINANT SPIKE PROTEIN

The S protein of SARS-CoV-2 has emerged as a highly relevant biotechnological tool not only for the development of vaccines and therapies but also for the investigation of the molecular mechanisms of diseases. It is a class I viral fusion homotrimer, whose S1 subunit contains the receptor-binding domain (RBD), which interacts with high affinity with Angiotensin-Converting Enzyme 2 (ACE2), allowing viral entry into the host cell (Figure 2). The production of this protein in a recombinant form, usually in expression systems, allows for the acquisition of pure and standardized quantities for in vitro studies. The seminal work of Wrapp *et al*. (2020) was fundamental in elucidating the cryo-electronic structure of the S protein, providing the structural basis for all subsequent studies that use it as an experimental tool.

In the context of neuroscience, the application of recombinant S protein has gained prominence for modeling the neurological consequences of infection, opening a new front of research to understand its potential relationship with neurodegenerative diseases, such as AD.

Considering that the ACE2 receptor is expressed in neurons, astrocytes, and microglial cells in the central nervous system, the direct exposure of these cells to recombinant S protein in vitro allows for the mimicking of key events of AD.

Recent evidence demonstrates that the S protein is capable of inducing a robust neuroinflammatory state, one of the pillars of AD. According to Oh *et al*. (2022), the recombinant S1 subunit triggers a pro-inflammatory response in microglia and astrocyte cultures, resulting in the significant release of cytokines such as interleukin-6 (IL-6) and tumor necrosis factor-alpha (TNF-α), as well as the generation of ROS. This chronic inflammatory environment is cytotoxic to neurons and contributes to the progression of neurodegeneration. Parallely, the recombinant spike can compromise the integrity of the blood-brain barrier (BBB), as demonstrated by Buzhdygan *et al*. (2020), who observed an increase in permeability in BBB cellular models after exposure to the protein. Dysfunctional BBB facilitates the entry of neurotoxic and inflammatory agents into the brain parenchyma, worsening the pathology.

In addition to neuroinflammation, more direct mechanisms linked to key AD proteins have been explored. Fontes-Dantas *et al*. (2023) presented evidence that the S protein can activate signaling pathways that lead to the hyperphosphorylation of tau protein, one of the pathological markers of neurofibrillary tangles. Additional studies, including in silico modeling such as that of Lyra *et al*. (2022), raise the hypothesis of an interaction between the Spike and the Cellular Prion Protein (PrPc), potentially interfering with the clearance of the Aβ peptide, although this relationship requires further experimental validation.

Therefore, recombinant protein S serves as a biologically relevant and precise stressor agent. By exposing neural cell cultures such as neuroblastoma cell lines, astrocytes, or microglia to specific concentrations and treatment times, it is possible to induce a cellular phenotype that recapitulates crucial aspects of AD: oxidative stress, inflammation, and protein dysfunction, thus offering an innovative approach of great clinical relevance in the post-pandemic scenario.

Figure 2 – Viral Entry Mechanism of Sars-CoV-2 thru the binding of the Spike protein to the Angiotensin-Converting Enzyme (ACE2).

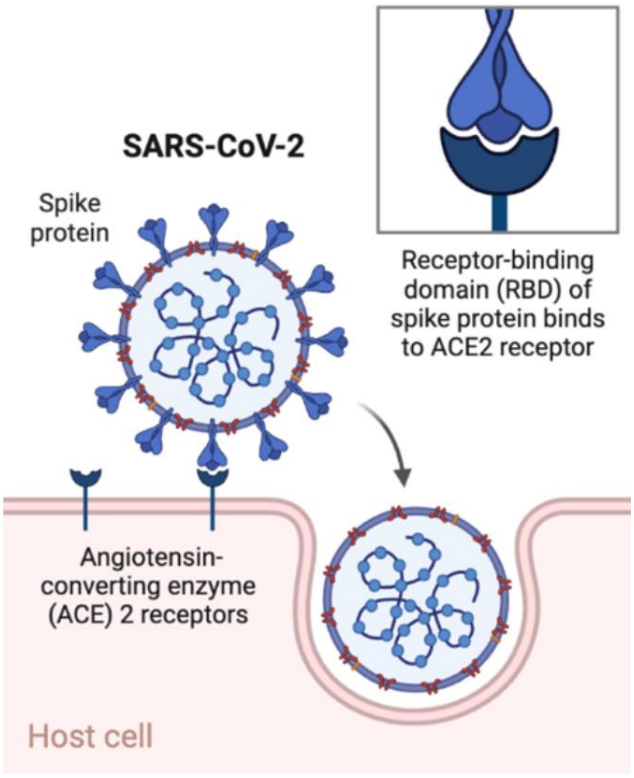

Source: Kruse, 2020.

3.5 PHOTOBIOMODULATION

PBM is a therapeutic modality that uses low-intensity light in the red (600 - 700 nm) and near-infrared (NIR; 780 - 1100 nm) spectra to induce beneficial cellular responses without causing significant thermal effects. Originally called low-level laser therapy (LLLT), PBM has been widely investigated in various medical fields, especially in neurology, due to its potential in treating neurodegenerative diseases, such as AD (Hamblin, 2019).

The main cellular chromophore responsible for the effects of PBM is cytochrome c oxidase (CCO), the complex IV of the mitochondrial electron transport chain. The absorption of photons by CCO promotes the dissociation of nitric oxide (NO), a physiological inhibitor of cellular respiration, resulting in an increase in mitochondrial membrane potential, ATP production, and ROS at low concentrations, which act as signaling molecules, a phenomenon known as mitohormesis (Freitas; Hamblin, 2016). This initial bioenergetic stimulus triggers a cascade of secondary signaling, culminating in the elevation of gene expression associated with cell survival, proliferation, cytoprotection, and modulation of the inflammatory response (Hamblin, 2017).

The choice of wavelength constitutes a critical parameter, as it determines the depth of tissue penetration. While red light is more effective in superficial tissues, IVP light exhibits lower absorption by skin components and greater penetration capability, reaching deep structures, including the cerebral parenchyma when applied transcranially (Tedford *et al*., 2015).

Preclinical evidence indicates that PBM can positively modulate the pathophysiological processes of AD, such as the accumulation of Aβ plaques, hyperphosphorylated tau protein neurofibrillary tangles, mitochondrial dysfunction, oxidative stress, and chronic neuroinflammation. In transgenic animal models of AD, the application of PBM with IVP (810 nm) significantly reduced the amyloid plaque load in the cortex and hippocampus (Purushothuman *et al*., 2014), possibly through the regulation of Aβ-degrading enzymes, such as neprilysin, and the improvement of glial clearance function, mediated by the increase of ATP (Grillo, 2023. Moreover, modulation of the innate immune response in the brain is observed, with a reduction in pro-inflammatory microglial activation (M1) and polarization toward an anti-inflammatory and phagocytic profile (M2), favoring the removal of protein aggregates and the release of neurotrophic factors (Yang *et al*., 2020a).

Moreover, recent studies have investigated the neuroprotective effects of PBM in cellular models related to AD. For example, Rossato *et al*. (2025) demonstrated that PBM associated with taurine promotes protection in SH-SY5Y cells subjected to oxidative stress induced by H_2O_2. These findings reinforce the potential of FBM as a promising therapeutic strategy for neurodegenerative diseases, corroborating the effects observed in international preclinical studies.

3.6 THREE-DIMENSIONAL CELL CULTURE

Traditional biomedical research has been largely based on 2D cell culture models, which, despite their simplicity and low cost, present significant limitations. These models fail to simulate the architectural complexity, cell-extracellular matrix (ECM) interactions, and biochemical gradients present in native tissues, resulting in cellular responses that often have low correlation with in vivo physiology. In contrast, 3D culture models emerge as a superior model, as they more faithfully mimic the tissue microenvironment, allowing multidirectional interactions and the formation of structures that more closely resemble the organization and function of real organs (Kapalczynska, 2018; Langhans, 2018).

The superiority of 3D models lies in their ability to replicate critical features of the in vivo microenvironment. One of the pillars of this advantage is the presence of a 3D ECM, which provides not only structural support but also a myriad of biochemical and mechanical signals that regulate fundamental cellular processes such as proliferation, differentiation, migration, and survival. Scaffold-based models, natural or synthetic hydrogels recreate this ECM, being especially useful for the generation of brain organoids that require support for the development of complex structures (Lancaster; Knoblich, 2014). This phenomenon, in which the cells inside an aggregate experience microenvironmental conditions distinct from those of the cells at the periphery, is a relevant physiological aspect for the study of cellular stress mechanisms and resistance, directly relevant to the pathogenesis of AD (Costa *et al*., 2016).

In the specific context of AD, the use of 3D models is not merely an improvement but a necessity. 2D models are not capable of reproducing the spatial deposition of the Aβ protein and the integrated glial response observed in the brain. 3D models, particularly spheroids formed by co-cultures of neurons and glial cells, allow the study of these multicellular interactions in a spatially organized context, generating more robust and translational pathological phenotypes (Park *et al*., 2018).

There are two main categories of 3D models applicable to AD research. The first are scaffold-based models, which use a support matrix, such as the already mentioned hydrogels, ideal for constructing highly customizable microenvironments. The second, and often more accessible, are scaffold-free models, such as spheroids. Spheroids are spherical and compact cellular aggregates formed spontaneously through cell-cell adhesion. They can be generated from neuronal cell lines or co-cultures, offering a robust model to study Aβ toxicity, neuroinflammation, and response to therapies (Costa *et al*., 2016).

The efficacy of PBM is closely linked to its tissue penetration and its interaction with mitochondrial cytochrome c oxidase. Thus, a 3D model, with its thickness and cellular density, imposes a barrier to light penetration much closer to physiological reality than a 2D monolayer. This allows for a more realistic evaluation of the dose and efficacy of PBM treatment in mitigating damage caused by factors such as oxidative stress and neuroinflammation within a microenvironment that recapitulates the complexity of neural tissue affected by AD (Yang, L. *et al.*, 2020b). In this way, 3D culture is not just a modeling tool but an essential component for generating biologically significant data with greater potential for clinical translation.

4 METHODOLOGY

4.1 STUDY LOCATION

This study was conducted at the Laboratory of Cellular and Tissue Biology - Dynamics of Cellular Compartments, under the coordination of Prof. Dr. Cristina Pacheco-Soares, affiliated with the Research and Development Institute (IP&D) of the University of Vale do Paraíba (UNIVAP), located in São José dos Campos, SP, Brazil

4.2 REAGENT AND EQUIPMENT

All reagents, chemicals, antibodies, supplements, and equipment were obtained from certified suppliers and handled according to the manufacturer's instructions to ensure reproducibility. The complete list of materials used in all cell culture workflows, differentiation, treatments, staining, imaging, and data analysis is presented in Table 2.

Table 1 - Reagents, supplements, equipment, and software used in the experimental procedures.

(continue…)

Reagent or resource	Source	Identifier
Reagents, antibodies, supplements, and other chemicals		
Agarose	Sigma-Aldrich, USA	9012-36-6
Anti- focal adhesion kinase **(**FAK**)** antibody	Cell Signaling Technology, USA	3285
DAPI	Sigma-Aldrich, USA	D9564
Dulbecco's modified Eagle's medium/nutrient mixture F-12 (DMEM/F12)	Gibco, USA	12400024
fetal bovine serum (FBS)	Gibco, USA	12657-029
Hydrogen peroxide (H_2O_2)	Molekular Química, Brazil	L0032-P1L
Paraformaldehyde	Sigma-Aldrich, USA	30525-89-4
Penicillin/streptomycin	Gibco, USA	15140-122
Phalloidin	Sigma-Aldrich, USA	49409
Phosphate-buffered saline (PBS)	Sigma-Aldrich, USA	806552
Recombinant SARS-CoV-2 Spike protein (S)	LECC – UFRJ, Brazil	LECC-COV2-AC001 (lot: O-151021)
Resazurin sodium salt	Sigma-Aldrich, USA	R7017
Retinoic acid (RA)	Sigma-Aldrich, USA	R2625
Triton X-100	Sigma-Aldrich, USA	9002-93-1
Trypsin – EDTA	Gibco, USA	15090046
MitoTracker™	Invitrogen, USA	M7510
Hoechst 33342	Invitrogen, USA	H3570
Plastics and other nonperishable materials		
cell culture flasks (25 cm^2)	Nest, China	707003
cell culture plates (24-well)	Kasvi, Brazil	K12-024
hive-patterned array	BioEdTech, Brazil	Bio3DStamp version 6
Equipment and software		
CO_2 incubator	Panasonic, Japan	MCO-170AICUV-PA
confocal laser scanning microscope	Leica, Germany	TCS SP8

Table 2- Reagents, supplements, equipment, and software used in the experimental procedures.

(conclusion)

GraphPad Prism 5.0	**GraphPad Inc., USA**	**Prism 5.0**
ImageJ Fiji	National Institutes of Health, USA	https://imagej.net/ij/
microplate reader	Bmg Labtech, Germany	VANTAstar
Scanning electron microscope	Zeiss, USA	EVO MA-10
Flow Cytometry	BD - Becton Dickinson	ACCURI C6 PLUS

Source: Author, 2025.

4.2 CELL LINE CULTURE

The human neuroblastoma cell line SH-SY5Y (ATCC® CRL-2266™) was used in this study. Cells were routinely cultured in 25 cm² cell culture flasks containing DMEM/F12 medium (Dulbecco's Modified Eagle Medium/Nutrient Mixture F-12), supplemented with 10% (v/v) fetal bovine serum and 1% (v/v) penicillin–streptomycin solution. Cultures were maintained in a humidified incubator at 37°C with 5% CO_2, and the culture medium was renewed every two days.

4.2.1 INDUCTION OF OXIDATIVE STRESS

Hydrogen peroxide (H_2O_2) was initially prepared as a 160,000 µM stock solution. Serial dilutions were subsequently performed in culture medium to obtain intermediate concentrations of 16,000 µM, 1,600 µM, 800 µM, and 400 µM. The final concentration of 200 µM was prepared by diluting the 400 µM solution, and this concentration was used in the experiments. The selection of this concentration was based on a previous study employing 2D and 3D neuronal models under oxidative stress conditions, in which exposure to 200 µM H_2O_2 was able to reproducibly induce oxidative stress without irreversibly compromising cell viability (Salles *et al.,* 2025).

All solutions were diluted in neuronal differentiation medium and prepared immediately prior to use to ensure compound stability. After five days of neuronal differentiation, cells assigned to the oxidative stress induction groups were exposed to 200 µM H_2O_2 for 1 hour in a humidified incubator at 37 °C with 5% CO_2.

4.2.2 EXPOSURE TO THE SPIKE PROTEIN

In this study, recombinant SARS-CoV-2 S protein was used, corresponding to amino acids 1–1208 of the sequence (full-length form). The protein was produced via recombinant technology at the Cell Culture Engineering Laboratory (LECC), COPPE/UFRJ (Rio de Janeiro, Brazil), using HEK 293 cells cultured in chemically defined medium, with purification performed by affinity chromatography.

Protein characterization was confirmed by SDS-PAGE and Western blot analyses, ensuring structural integrity and immunoreactivity. Detailed information regarding concentration, purity, stability, and characterization assays is described in the Certificate of Analysis provided by LECC (Annex A).

The batch used (O-151021) was supplied in phosphate-buffered saline (PBS) containing biotin, with a total concentration of 0.250 mg/mL and preserved with 0.02% (w/v) sodium azide. For the experiments, the protein was used at a final concentration of 0.5 µg/mL, diluted in cell differentiation medium.

The concentration was selected based on previous studies that employed similar values in different non-neuronal cell models, including human microglia (HMC3), endothelial cells, and in vitro blood-brain barrier models, in which alterations related to cell viability, mitochondrial integrity, and barrier permeability were observed (Buzhdygan *et al.,* 2020; Clough *et al*., 2021). Although specific studies using this exact concentration in neuronal lineages were not found, the choice of 0.5 µg/mL in this work sought to align with protocols previously established in the literature, ensuring the comparability and biological relevance of the results.

For the group exposed exclusively to the Spike protein, it was added directly to the wells containing differentiation medium. In the groups subjected simultaneously to oxidative stress induction and spike protein exposure, the protein was diluted directly into the medium containing H_2O_2. In both cases, cells were incubated for 1 h at 37°C in a humidified atmosphere with 5% CO_2. After the incubation period, the medium was replaced with complete culture medium, and the cells remained incubated for an additional 24 h prior to analysis.

4.3 FABRICATION OF 3D MOLDS

The molds were fabricated from an ultrapure agarose solution, previously autoclaved and dissolved in 1x PBS. The final agarose concentration was 2% (w/v). For preparation, agarose powder was added to PBS in flasks with double the capacity of the total solution volume to prevent overflow and loss by evaporation. The mixture was heated in a microwave with the

cap slightly loosened (in Schott-type flasks) in 30-second cycles until complete dissolution and the attainment of a homogeneous and translucent solution.

After the complete melting of the agarose, the container was transferred to a laminar flow hood for subsequent sterile handling. The resin molds (3D devices) used as stamps were previously sanitized with 70% alcohol and exposed to ultraviolet (UV) radiation for 15 minutes.

To form the molds, 2 mL of the still-hot agarose solution were added to the wells of 12-well plates, filling the bottom uniformly. Subsequently, the 3D devices were carefully inserted at a slight angle to avoid the formation of air bubbles and to ensure complete filling of the gaps between the micro-wells. Gelation was carried out at room temperature for approximately 20 to 30 minutes, accelerated with the aid of artificial ice (gel pack) positioned under the plate on a flat surface.

The complete formation of the molds was visually confirmed by the opacification of the agarose. After solidification, the stamps were cautiously removed. To ensure the sterility of the molds, a layer of 70% alcohol was applied over the wells containing the solidified agarose, followed by a new exposure to UV radiation for 15 minutes.

4.4 MOLDS MATURATION AND PH EQUILIBRATION

Prior to cell seeding, the agarose molds underwent a maturation process to equilibrate the pH and ensure adequate hydration of the matrix. For this purpose, complete culture medium was added to each well containing the molds, followed by a 15-minute incubation. Subsequently, the liquid was removed and replaced with fresh culture medium, repeating the process for three successive washes, with a 15-minute incubation between each exchange. After equilibration, the medium was completely removed before seeding the cell suspension.

If the molds were not used immediately, they were kept hydrated with 1x PBS and stored in an incubator at 37 °C to prevent dehydration and potential alterations in the microwell dimensions.

4.5 CELL SEEDING AND NEURONAL DIFFERENTIATION

Upon reaching approximately 80% confluence in culture, SH-SY5Y cells were trypsinized and seeded. For the assays, seeding was performed in 24-well plates at a density of $1x10^5$ cells/mL, divided into two plates: one to evaluate the therapeutic effects of irradiation (PBM) and the other as a non-irradiated control. Once seeded, the monolayer cultures remained

for 2 days in complete medium (as described in section 4.2), while the three-dimensional cultures remained for 5 days. Subsequently, the cells underwent neuronal differentiation for an additional 5 days in medium containing 10 µM retinoic acid, 0.5% Fetal Bovine Serum (FBS), and 1% Penicillin/Streptomycin, diluted in DMEM/F12. The cells, now differentiated into a neuronal model, were divided into 7 groups as described in Table 3.

Table 2 – Experimental groups and corresponding treatments

Group	Treatment
Control	Differentiated SH-SY5Y cells without additional treatment.
Oxidative Stress (H_2O_2)	Exposure to 200 µM H_2O_2 for 1 h.
PBM	PBM (660 nm, 3 J/cm²).
H_2O_2 + PBM	H_2O_2 (200 µM, 1 h) followed by PBM (660 nm, 3 J/cm²).
S protein	Treatment with recombinant S protein (0.5 µg/mL) for 1 h.
S protein + PBM	S protein (0.5 µg/mL, 1 h) followed by PBM (660 nm, 3 J/cm²).
H_2O_2 + S protein	Simultaneous exposure to H_2O_2 (200 µM) and S protein (0.5 µg/mL) for 1 h.
H_2O_2 + S protein + PBM	Combined exposure to H_2O_2 (200 µM) and S protein (0.5 µg/mL) for 1 h, followed by PBM (660 nm, 3 J/cm²).

Source: Author, 2025.

4.6 IRRADIATION

Following the exposure period to H_2O_2 and/or the Spike (S) protein, the groups designated to receive PBM were subjected to the irradiation protocol. The light source used was a light-emitting diode (LED) device with a wavelength of 660 nm (red spectrum).

The procedure was performed in an environment with controlled lighting. The culture plates were positioned under the LED emitter, ensuring that the surface of the culture medium was perpendicular to the light source to guarantee a uniform and reproducible energy dose across the cell monolayer. The exposure time was 1 minute and 22 seconds, resulting in a total energy dose (fluence) of 3 J/cm².

4.7 CELL VIABILITY

4.7.1 ALAMARBLUE ASSAY

Cell viability was evaluated, after irradiation, by means of the metabolism assay with AlamarBlue, a redox indicator that undergoes reduction by mitochondrial dehydrogenases of metabolically active cells.

The executed protocol consisted of replacing the culture medium of each well with a solution containing 90% (v/v) of neuronal differentiation medium and 10% (v/v) of the AlamarBlue reagent. The plates were then incubated for 2 hours in an incubator at 37°C and

5% CO_2, protected from light. After the incubation period, a 100 µL aliquot of the solution from each well was transferred to a 96-well plate. The fluorescence of the reduced product was measured through a fluorescence reading in a microplate reader from the Nanosensors Laboratory of the Institute of Research and Development/Univap, using a 544 nm excitation filter and a 590 nm emission filter.

The fluorescence values obtained for the experimental groups were normalized in relation to the control group (group i, neuronal cells), expressed as a percentage of cell viability. All determinations were performed in triplicate to ensure the reliability and reproducibility of the data.

4.7.2 VIABILITY AND APOPTOSIS ASSESSMENT BY FLOW CYTOMETRY (LIVE/DEAD)

For the quantification of live cell populations and those in the process of programmed death, flow cytometry analysis was performed using combined staining of Annexin V-FITC and Propidium Iodide (PI). This assay is based on the affinity of Annexin V for phosphatidylserine exposed on the outer face of the plasma membrane during the initial phases of apoptosis, while PI, a DNA-intercalating dye non-permeable to the membrane, penetrates only cells with compromised cytoplasmic integrity, allowing the identification of apoptosis stages.

After the experimental treatments, which included exposure to the Spike protein, H_2O_2 and PBM irradiation, the cells were detached and resuspended in Annexin Binding Buffer containing Ca^{2+}; the samples were initially incubated with Annexin V-FITC for 15 minutes at room temperature and under protection from light, followed by the addition of PI 5 minutes before the reading. It is important to highlight that the cells were not subjected to the fixation process, ensuring the fidelity of the viability marking in real-time.

Data acquisition was conducted on a BD Accuri™ C6 flow cytometer, part of the Multi-user Central of the Institute of Research and Development (IP&D), with the collection of at least 10,000 events per sample. The analysis strategy consisted of the exclusion of cellular debris and the selection of singlets through light scattering parameters (FSC vs. SSC). The discrimination of subpopulations was performed through scatter plots (dot plots) correlating the FL1 (Annexin V) and FL3 (PI) channels, allowing classification into live cells (Annexin V-/PI-), early apoptosis (Annexin V+/PI-), and late apoptosis or necrosis (Annexin V+/PI+). To

ensure analytical precision, spectral compensation controls and biological controls were applied for the validation of the markings.

4.8 MITOCHONDRIAL AND NUCLEAR ANALYSIS

The evaluation of the integrity and mitochondrial membrane potential and nucleus was performed using the fluorescent dye MitoTracker™ Orange CMTMRos, a probe that actively accumulates in the mitochondria of live cells as a function of membrane potential, and the Hoechst dye for nuclear marking. A 1 μM working solution of the MitoTracker™ dye in neuronal differentiation medium was prepared. This solution was added to each well and the plates were incubated for 30 minutes in an incubator at 37 °C with 5% CO_2, protected from light.

After the incubation period, the samples were prepared for analysis in a laser confocal microscope, being washed three times with 1x PBS. Image acquisition was performed using excitation filters of 552 nm and emission of 576 nm for MitoTracker, and excitation of 353 nm and emission of 454 nm.

4.9 CELL ADESION AND CYTOSKELETON ANALYSIS

In addition to the experiments conducted under oxidative stress conditions (treatments with H_2O_2, Spike, and LED), an additional set of analyses was conducted on differentiated SH-SY5Y cells, not subjected to stress, with the objective of specifically evaluating the direct effect of the S protein on cell adhesion and cytoskeleton organization in 2D. For this, the cells were cultivated under identical conditions to those described previously and exposed or not to the S protein, being subsequently marked with phalloidin (for visualization of the actin network) and an antibody against the FAK protein (focal adhesion kinase). These experiments had a complementary character and allowed for the isolated evaluation of the spike's action on basic structural parameters of the differentiated neuronal cells.

For the analysis of cytoskeleton organization and nuclear marking, the cells were fixed with 4% paraformaldehyde (PFA) in PBS for 20 minutes at room temperature, washed gently in PBS, and permeabilized with 0.1% Triton X-100 for 10 minutes. Subsequently, the samples were washed twice in PBS and incubated overnight at 4°C and protected from light with a solution containing rhodamine-phalloidin (1:500) (49409, Sigma-Aldrich, St. Louis, USA) and DAPI (1:5000) (D9564, Sigma-Aldrich, St. Louis, USA), diluted in PBS. After incubation, two

additional washes with PBS were performed, and the samples were prepared for analysis in a confocal microscope.

For FAK marking, after fixation and permeabilization as described previously, the samples were incubated with a primary anti-FAK antibody (rabbit species) diluted in PBS for 1 hour at 37°C. After three washes in PBS, incubation with a conjugated anti-rabbit secondary antibody proceeded, also for 1 hour at 37°C, protected from light. Finally, the samples were analyzed by confocal microscopy. All incubation parameters, dilutions, and acquisition conditions were properly standardized to ensure the reproducibility of the experiments.

4.10 SCANNING ELECTRON MICROSCOPY

For the morphological analysis of the samples, these were processed for scanning electron microscopy (SEM) using a protocol based on dehydration through an increasing series of solvents and drying with hexamethyldisilazane (HMDS). Initially, the samples were washed in PBS and, subsequently, subjected to sequential dehydration in increasing concentrations of acetone (or ethanol) of 30%, 50%, 70%, and 100%, remaining for 10 minutes in each solution. After this step, the samples were incubated for 10 minutes in a 1:1 solution of acetone and HMDS, followed by incubation in 100% HMDS until complete evaporation, allowing the drying of the structures. Subsequently, the dried specimens were mounted on metallic stubs using conductive carbon tape, metallized with a thin layer of gold in a sputter coater, and analyzed in a scanning electron microscope.

4.11 STATISTICAL ANALYSIS

The data obtained were tabulated and analyzed using GraphPad Prism software, version 5.0 (GraphPad Software Inc., San Diego, CA, USA). All experiments were performed in three independent technical replicates per experimental condition, and the results were expressed as mean ± standard deviation (SD). For the comparison of means between the different experimental groups in cell viability assays (Alamar Blue) and in flow cytometry parameters (Live/Dead), one-way Analysis of Variance (ANOVA) was used, followed by Tukey's post-test for multiple comparisons.

5 RESULTS AND DISCUSSION

5.1 STANDARDIZATION OF THE NEURONAL THREE-DIMENSIONAL MODEL (SH-SY5Y SPHEROIDS)

The achievement of homogeneous and viable spheroids from differentiated SH-SY5Y cells represents an important advancement in the in vitro modeling of neurodegenerative processes. Cultivation in neuronal medium allowed the formation of stable, spherical, and homogeneously sized structures after approximately seven days (Figure 3). Initially, the cells appeared highly compacted, with no evident central necrosis, which indicates adequate diffusion of nutrients and oxygen. This morphological pattern was fundamental for the standardization of the model, given that structural stability is the primary requirement for subsequent investigations (Salles *et al*., 2025).

Figure 3 - Stages of SH-SY5Y cell spheroid formation in brightfield. From left to right: monolayer culture (2D Cells); initial sedimentation and aggregation phase in agarose microwells (Seeded Cells); and the finalized three-dimensional model (Spheroids), showing high compactness and homogeneous structural organization after 7 days of cultivation.

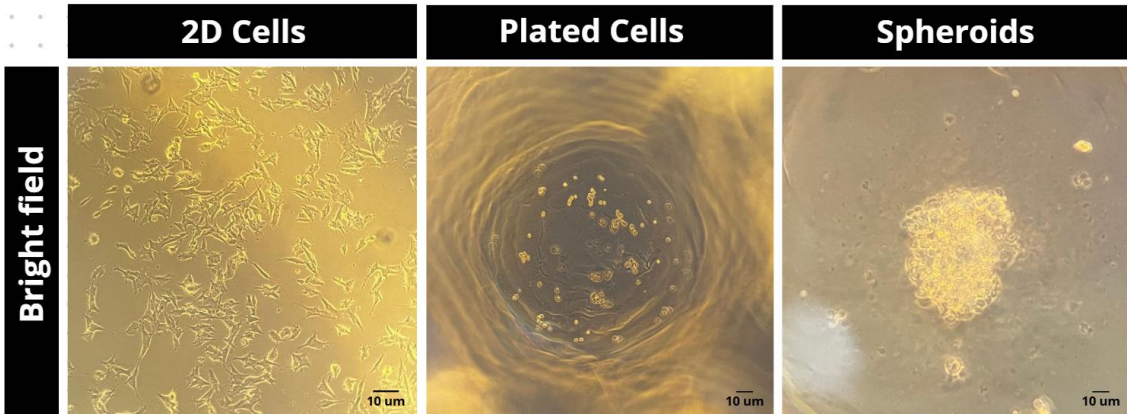

Source: Author, 2025.

Unlike 2D cultures, 3D systems offer superior complexity, reproducing with greater fidelity the cell-cell and cell-matrix interactions present in nervous tissue. This organization favors the maintenance of differentiated neuronal phenotypes and allows for a more realistic evaluation of the cellular response to toxic or therapeutic stimuli. The validation of this sensitivity was confirmed by exposure to H_2O_2, which promoted functional alterations and the loss of spheroid compactness. This finding suggests that hydrogen peroxide compromised cell adhesion and cytoskeletal integrity through the generation of ROS, inducing mitochondrial dysfunction and activating apoptotic pathways (Fan; Hussien; Brooks, 2010).

Scanning Electron Microscopy (SEM) analysis provided additional evidence regarding the model's susceptibility to the spike protein. Spheroids exposed to the viral protein exhibited a loss of cellular compactness and a marked irregularity in the outer border, which assumed a rough and heterogeneous appearance (Figure 4). Compared to the 2D model, in which treatment resulted only in reduced viability and monolayer alterations, the 3D model revealed an additional phenotype of structural retraction and loss of tissue integrity. This phenomenon is a central characteristic of neurodegenerative diseases, such as Alzheimer's, indicating that spheroids can mimic more advanced stages of the degenerative process.

Figure 4 - Structural analysis by Scanning Electron Microscopy (SEM) of SH-SY5Y neural spheroids. The panels on the left present the organization of the spheroids arranged in agarose microwells, while the panels on the right exhibit the surface morphology at higher magnification. (Control Group): High cellular compaction, architectural integrity, and a regular outer surface are observed, characteristic of stable and cohesive three-dimensional models. (Exposed Group): Exposure to the SARS-CoV-2 spike protein resulted in loss of cellular compactness and irregularity in the outer border of the spheroid, which assumed a rough and heterogeneous appearance, indicating impairment of adhesion and structural organization after the viral challenge.

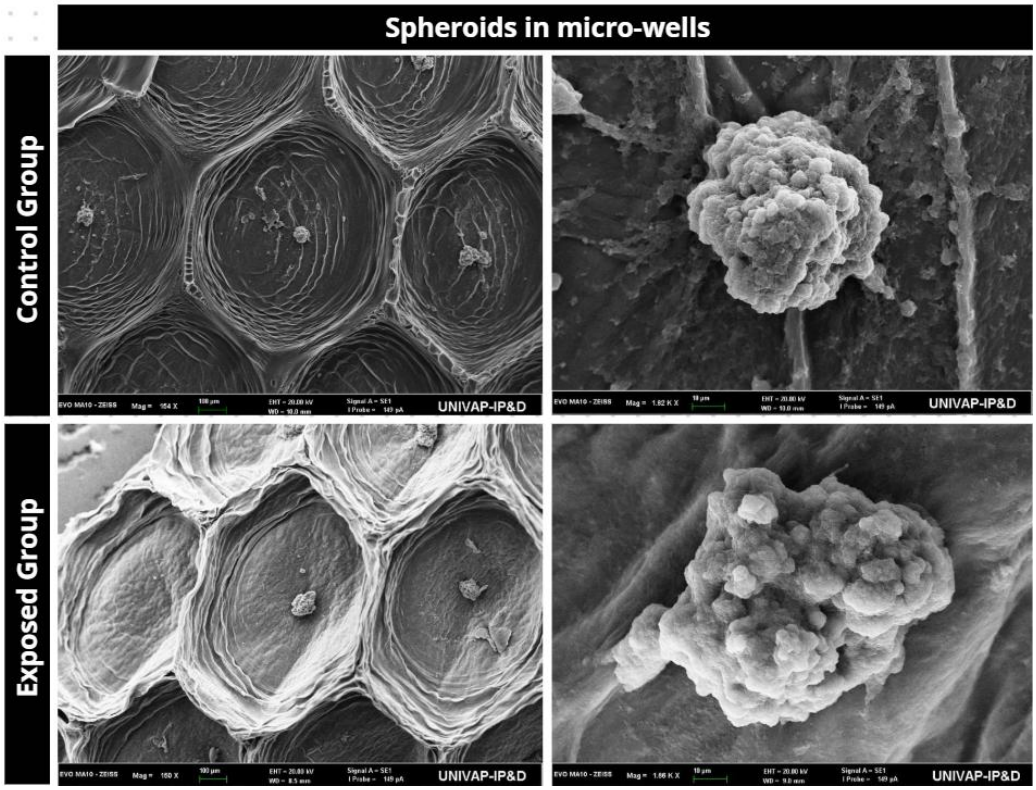

Source: Author, 2025.

Another relevant differentiator is the presence of nutrient and oxygen gradients inherent to the 3D structure. Unlike 2D culture, where exposure to the medium is uniform, the impact of stressing agents on the spheroids occurs heterogeneously between the outer and inner layers. This explains the observation of central regions with lower cell density and signs of apoptosis under intense stress. Therefore, the standardized 3D model proves to be suitable not only for

reproducing the effects of oxidative stress and viral toxicity in differentiated neurons but also for studying the interaction between morphological and metabolic events. In short, this system establishes a robust platform for the evaluation of neuroprotective therapies, such as photobiomodulation (PBM), significantly increasing the translational relevance of the findings obtained.

5.2 CELL VIABILITY AND METABOLIC EFFECTS IN NEURONAL MODELS

5.2.1 EVALUATION OF METABOLIC VIABILITY BY ALAMAR BLUE

The analysis of cell viability, expressed as a percentage of the respective control group, revealed distinct responses between the two-dimensional (2D) and three-dimensional (3D) models of differentiated neurons (Figures 5 and 6). In the 2D model, it was observed that H_2O_2-induced oxidative stress promoted a sharp reduction in cell viability, evidencing its significant cytotoxic effect (****$p < 0.0001$). Exposure to the spike protein alone also resulted in a significant reduction in metabolic viability, with values around 80% of the control (****$p < 0.0001$), indicating that the viral protein, even in the absence of oxidative stress, compromises the metabolic activity of cells in this model. The association between the Spike protein and H_2O_2 in the 2D model maintained values close to those of the group exposed only to H_2O_2 (****$p < 0.0001$). Although the metabolic activity was similar between these two groups, morphological analyses demonstrated that the Spike protein + H_2O_2 group presented more severe structural alterations, with a reduction in the number of intact nuclei and greater nuclear fragmentation, suggesting a functional and morphological synergistic effect between the viral protein and oxidative stress.

Figure 5 - Cytoviability of 2D neuronal cells model following exposure to Spike protein and/or H_2O_2-induced oxidative stress, with or without PBM. Cell viability is expressed as a percentage relative to the corresponding control group after treatment with H_2O_2 (200 µM), Spike protein (0.5 µg/mL), or their combined exposure (Spike + H_2O_2). Data are presented as mean ± standard deviation. Groups were evaluated 2 h post-irradiation (660 nm, 3 J/cm²). PBM significantly mitigated the cytotoxic effects induced by Spike protein exposure, preserving neuronal viability. Statistical significance compared with the respective control group is denoted by *** ($p < 0.001$), **** ($p < 0.0001$) and ns nonsignificative.

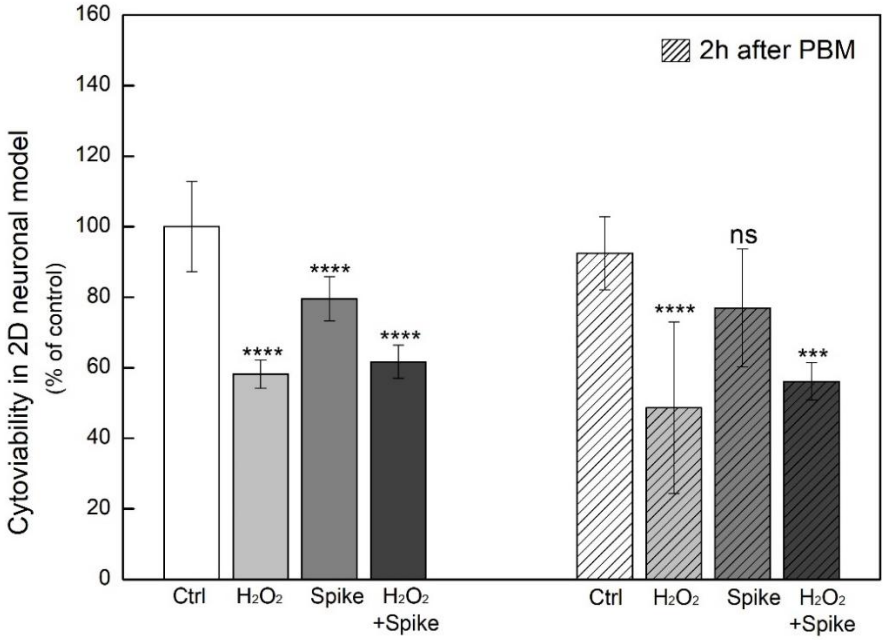

Source: Author, 2025.

These results corroborate the literature describing H_2O_2 as a potent inducer of oxidative stress, promoting mitochondrial dysfunction and the activation of apoptotic pathways (Fan; Hussien; Brooks, 2010; Salles *et al*., 2025). In the case of the Spike protein, studies indicate that its interaction with cellular receptors can deregulate the focal adhesion pathway mediated by FAK, impairing survival signals (Simons *et al*., 2021). In the 2D model, the application of PBM by LED did not result in a statistically significant recovery of metabolic viability in the groups under stress, although the literature suggests that PBM can modulate mitochondrial metabolism via cytochrome c oxidase (Hamblin, 2017; Salehpour *et al*., 2018).

In parallel, the evaluation in the three-dimensional model (Figure 6) revealed a distinct metabolic response pattern dependent on the cellular architecture (Figure 6). Exposure to H_2O_2 alone promoted a reduction in viability (**$p < 0.01$), confirming the sensitivity of the 3D system to oxidative stress. However, differently from what was observed in the 2D model, exposure to the Spike protein alone resulted in a significant increase in metabolic viability, with values higher than the control (**$p < 0.01$). Significantly, the combination of Spike protein + H_2O_2 in the 3D model also showed significantly higher viability when compared to the group exposed only to H_2O_2, suggesting that the presence of the Spike protein altered the metabolic response

to oxidative stress in this complex environment. This 3D organization confers greater functional resistance due to cell-cell interactions and physiological oxygen gradients (Edmondson *et al*., 2014; Ravi *et al*., 2015).

Figure 6- Cytoviability of 3D neuronal cells model following exposure to Spike protein and/or H_2O_2-induced oxidative stress, with or without PBM. Cell viability is expressed as a percentage relative to the corresponding control group after treatment with H_2O_2 (200 µM), Spike protein (0.5 µg/mL), or their combined exposure (Spike + H_2O_2). Data are presented as mean ± standard deviation. Groups were evaluated 2 h post-irradiation (660 nm, 3 J/cm²). Spike protein exposure within the 3D microenvironment increased cell viability. Under PBM, no statistical difference was observed between groups. Statistical significance compared with the respective control group is denoted by ** ($p < 0.01$), ns nonsignificative.

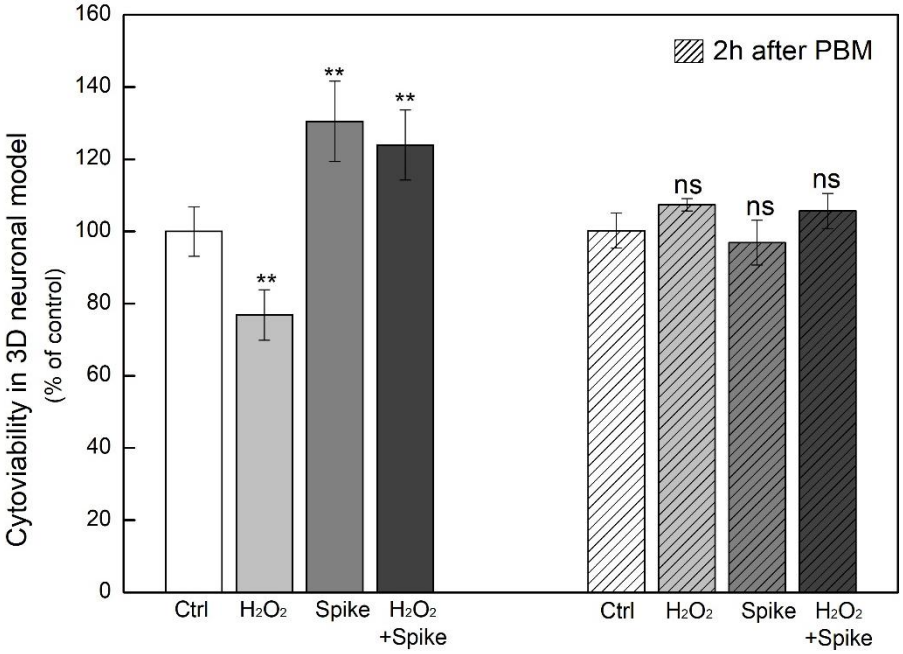

Source: Author, 2025.

The application of PBM in the 3D model demonstrated a regulatory effect on metabolic homeostasis. In the stressed groups that received LED (H_2O_2 + LED and Spike protein + H_2O_2 + LED), viability stabilized at levels close to the control, with no statistically significant difference, suggesting that irradiation contributed to normalizing cellular metabolic activity in the face of the induced damages (Hamblin, 2017; Salehpour *et al*., 2018). The differences observed between the models reinforce the influence of architecture on the response to stimuli. The increase in metabolic viability induced by the Spike protein in the 3D model may reflect a compensatory activation or an exacerbated metabolism resulting from the attempt to repair cellular damage (Erikstein *et al*, 2010). Previous studies demonstrate that SARS-CoV-2 proteins can alter mitochondrial function, promoting transient increases in metabolic activity that do not necessarily reflect a real increase in survival (Codo *et al*., 2020; Singh *et al*., 2020).

Taken together, the viability results provide a consistent basis for the subsequent morphological analyses, allowing for the correlation of metabolic alterations with the structural damages identified in the cytoskeleton and cell adhesion mechanisms. The 3D model emerges, therefore, as a critical system for capturing the modulations of COVID-19 neuropathogenesis, highlighting phenomena of cellular compensation and structural collapse that conventional 2D models may mask (Edmondson *et al*., 2014; Ravi *et al*., 2015).

5.2.2 CYTO-VIABILITY ANALYSIS BY FLOW CYTOMETRY (LIVE/DEAD)

Flow cytometry analysis allowed for the quantification of subpopulations of live cells and those undergoing apoptosis, providing a detailed view of cell survival dynamics that complements the metabolic viability data obtained by the Alamar Blue assay (Figure 7). The results showed that the control group presented the highest percentage of live cells, with insignificant levels of apoptotic marking, attesting to the stability and integrity of the initial neuronal model before the imposed damages. On the other hand, isolated exposure to hydrogen peroxide resulted in the sharpest reduction in the live cell population among the non-irradiated groups. This finding confirms the strong cytotoxicity of H_2O_2, which acts as a potent inducer of oxidative stress, promoting irreparable damage to the cytoplasmic membrane and mitochondrial dysfunction (Salles *et al*., 2025).

Figure 7– Viability and apoptosis analysis by flow cytometry in a 3D neuronal model. The populations of live and apoptotic cells were quantified after exposure to H_2O_2 (200 µM) and the Spike protein (0.5 µg/mL), treated or not with PBM (660 nm, 3 J/cm^3). The bars represent the mean ± SD of the cell percentage. It is noted that the spike protein alone induced the highest rate of apoptosis, yet exerted a cytoprotective effect against H_2O_2 in the combined exposure. PBM promoted the maintenance of viability and reduction of apoptosis in all groups under stress, affirming its neuroprotective potential.

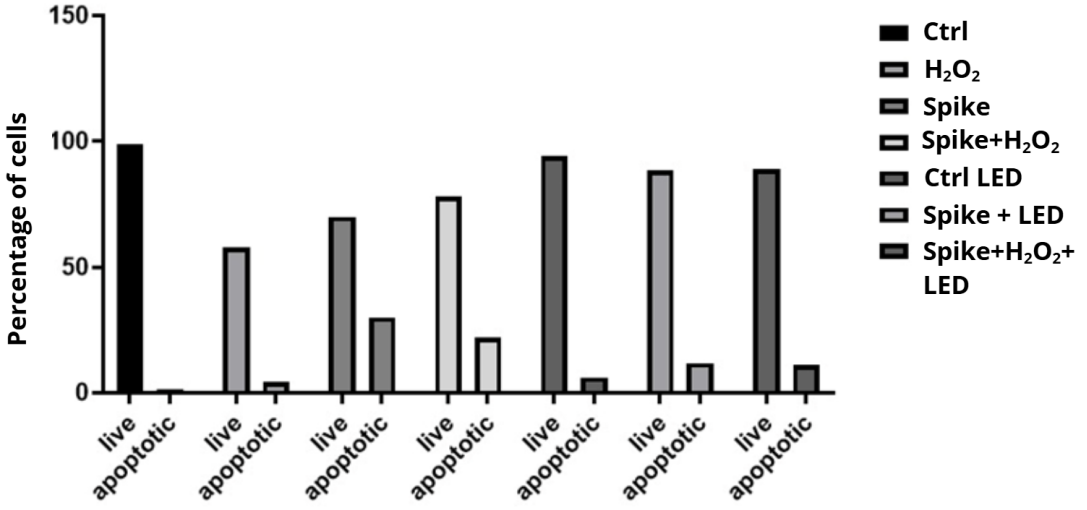

Source: Author, 2025.

Significantly, the group exposed only to the spike protein presented a higher population of live cells compared to the group subjected to isolated oxidative stress, although it recorded the highest rate of cells in the apoptotic stage compared to the other experimental groups. Furthermore, in the combined exposure group (Spike + H_2O_2), a higher percentage of live cells was observed than in the group treated only with H_2O_2, suggesting that the presence of the Spike protein exerted a cytoprotective or adaptive effect against severe oxidative stress. This phenomenon can be interpreted as an early adaptive response or cellular hormesis (Calabrese; Mattson, 2017), in which the initial stimulus from the spike protein activates pro-survival signaling pathways, possibly mediated by metabolic compensation mechanisms and phenotypic reprogramming, preparing the cell for subsequent oxidative stress. However, the increased apoptosis marking in the isolated spike group suggests that this response represents an exacerbated metabolic activation that precedes a more pronounced functional loss in the long term, as observed in the morphological analyses of structural collapse (Kroemer *et al*., 2009).

The application of PBM with 660 nm LED promoted an evident preservation of cell populations in all tested scenarios. In the irradiated groups (LED, Spike + LED, and Spike + H_2O_2 + LED), the percentage of live cells remained high and stable, with a drastic reduction in apoptosis markers compared to their respective non-irradiated counterparts under stress. This neuroprotective effect corroborates the classical mechanism of PBM on Cytochrome C Oxidase, which optimizes ATP production and stabilizes the mitochondrial membrane potential, preventing the progression of the apoptotic cascade and maintaining cell membrane homeostasis (Hamblin, 2017; Salehpour *et al*., 2018). Taken together, the flow cytometry data reinforce the hypothesis that the Spike protein modulates neuronal function in a contextual and adaptive manner, while PBM acts as a potent normalizing agent of cell survival in the face of viral and oxidative insults.

5.3 ALTERAÇÕES NUCLEARES E INTEGRIDADE CELULAR

The micrographs revealed striking differences between the experimental groups. In the two-dimensional model (Figure 8), the control group presented intact nuclei, with homogeneous distribution and preserved morphology. In the group exposed to the spike protein, a moderate reduction in the number of nuclei was observed, accompanied by early signs of chromatin condensation. In the groups subjected to oxidative stress, especially the Spike + H_2O_2 group, the nuclei appeared less numerous, intensely condensed, and, in some cases, fragmented—

morphological characteristics compatible with the activation of apoptotic processes induced by intense oxidative stress.

In contrast, the groups treated with PBM (Spike + LED; H_2O_2 + LED; Spike + H_2O_2 + LED) presented partial preservation of nuclear integrity, evidenced by less condensed nuclei, with more distributed chromatin and more homogeneous morphology compared to the non-irradiated groups under stress. These findings indicate that, although the LED did not completely reverse the induced damage, there was a clear attenuation of the nuclear alterations associated with oxidative stress and exposure to the spike protein.

Figure 8 – Micrographs of differentiated neuronal nuclei, non-irradiated (top row) and irradiated with PBM (bottom row) in a 2D model under the following conditions: Control, H_2O_2, Spike, and Spike + H_2O_2 stained with DAPI. Control cells exhibited uniformly distributed nuclei with preserved morphology. H_2O_2 induced chromatin condensation and nuclear fragmentation (red arrow). Cells exposed to the spike protein showed reduced nuclear density and moderate chromatin condensation (yellow arrow). The Spike + H_2O_2 group exhibited severe nuclear damage. The groups treated with PBM exhibited nuclei with less condensation and better structural preservation. Scale bars: 10 µm.

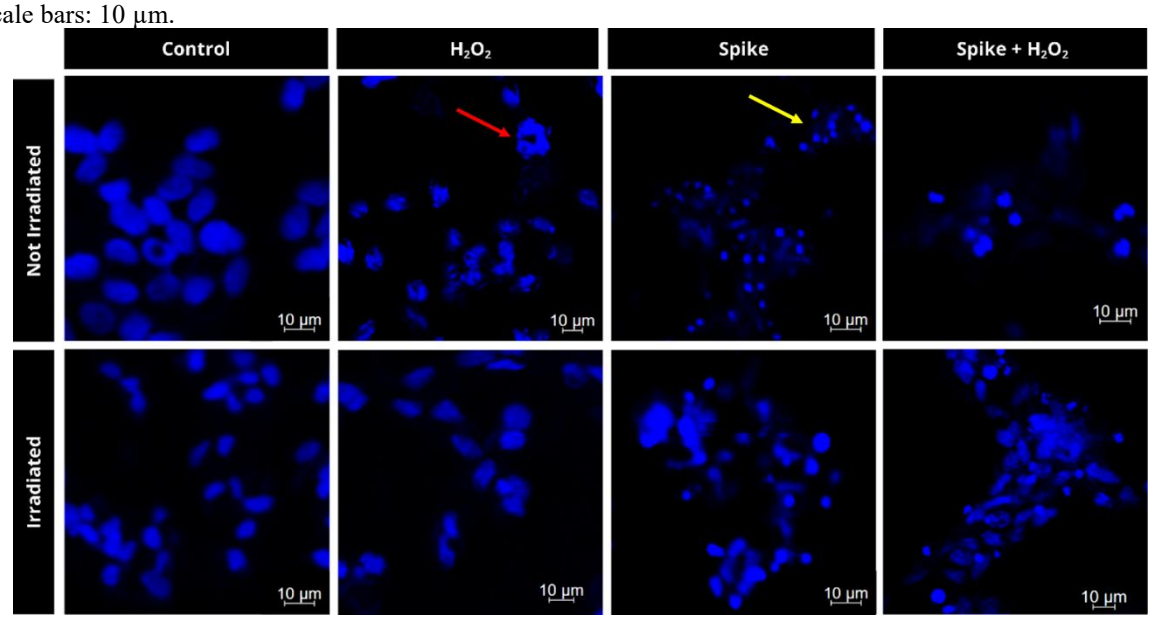

Source: Author, 2025.

The nuclear alterations observed in the groups treated with H_2O_2 are in agreement with the literature, which describes oxidative stress as a potent inducer of DNA damage, chromatin condensation, and nuclear fragmentation, classic events associated with apoptosis (Fan; Hussien; Brooks, 2010). The presence of intensely condensed and fragmented nuclei in the Spike + H_2O_2 group suggests that the combination of these insults potentiates cell death mechanisms, reinforcing the hypothesis of a synergistic effect between the viral protein and oxidative stress.

In the case of the isolated Spike protein, the moderate reduction in the number of nuclei, associated with early signs of condensation, suggests the activation of sublethal cellular stress

mechanisms. Previous studies indicate that the spike protein can interfere with signaling pathways related to cell adhesion and survival, leading to progressive structural changes without necessarily inducing immediate cell death (Rhea *et al*., 2021). This pattern is compatible with the findings observed in this study, in which the nuclei remain mostly intact, although they already show early signs of impairment.

The partial preservation of nuclear integrity in the LED treated groups can be interpreted in light of the effects of PBM on cellular homeostasis. The literature describes that PBM is capable of reducing oxidative DNA damage, modulating caspase activity, and attenuating apoptotic processes, especially through the stabilization of mitochondrial function and the reduction of excessive production of reactive oxygen species (Salehpour *et al*., 2018; Hamblin, 2016). Thus, the observation of less condensed nuclei with more homogeneous chromatin in the irradiated groups suggests that the LED contributed to the maintenance of nuclear integrity against the experimental insults.

These findings find direct support in the results obtained from the mitochondrial analysis (item 5.4), since mitochondrial dysfunction and the release of pro-apoptotic factors are closely associated with chromatin condensation and nuclear fragmentation. Thus, the data suggest that the partial protective effect observed in the nucleus occurs, at least in part, as a consequence of the preservation of mitochondrial function and the attenuation of the activation of oxidative stress-dependent apoptotic pathways.

The analysis of nuclear alterations in the three-dimensional model evidenced striking differences in organization, density, and nuclear integrity between the experimental groups (Figure 9), reflecting cellular responses dependent on both the type of stimulus and the application of PBM. In the non-irradiated control group, the spheroids presented high nuclear density, with nuclei compactly and homogeneously distributed throughout the three-dimensional structure. The nuclei exhibited rounded morphology, well-defined contours, and intense fluorescent signal, a characteristic pattern of viable and structurally organized 3D models, in which cell-cell interactions contribute to the maintenance of nuclear integrity and the neuronal phenotype (Edmondson *et al*., 2014; Ravi *et al*., 2015).

Figure 9 - Micrographs of differentiated neuronal nuclei, non-irradiated (top row) and irradiated with PBM (bottom row) in a 3D model under the following conditions: Control, H_2O_2, Spike, and Spike + H_2O_2. In the control group, high cell density with intact nuclei and compact distribution is observed, typical of stable three-dimensional organization. Exposure to H_2O_2 resulted in loss of spheroid compaction and signs of nuclear fragmentation. In the Spike group, a partial maintenance of the architecture is noted, although with slight heterogeneity in nuclear morphology. The Spike + H_2O_2 group exhibited the most severe impairment, with a significant reduction in nuclear density and disintegration of the spheroid structure. The irradiated groups (bottom row) demonstrated partial preservation of structural integrity and a higher density of intact nuclei compared to their respective non-irradiated counterparts, suggesting a protective effect of PBM on the organization of the 3D model. Scale bars: 10 µm.

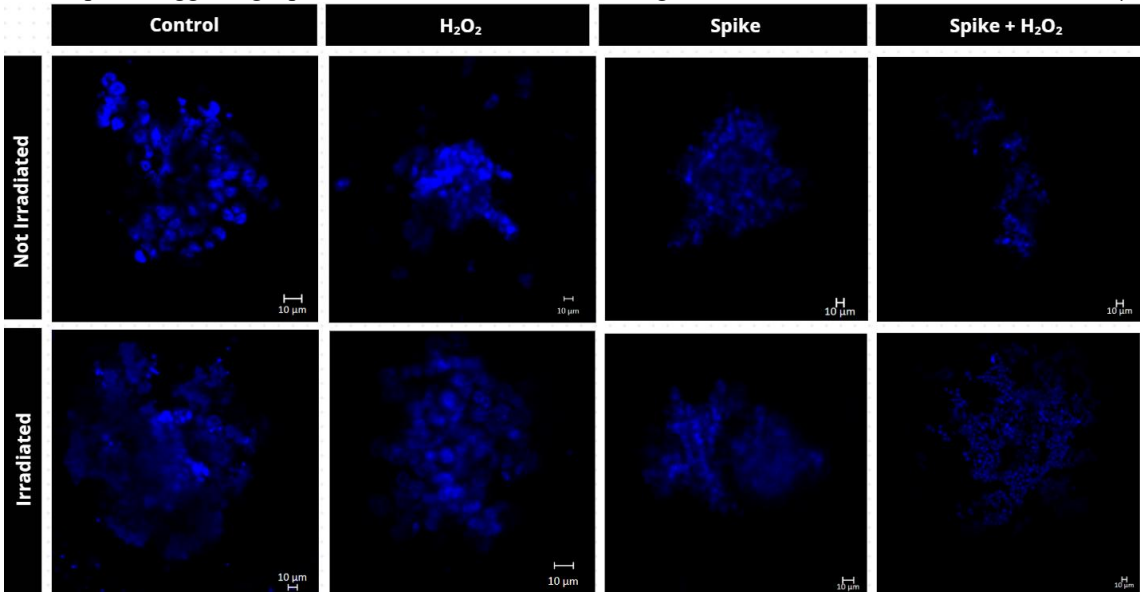

Source: Author, 2025.

Exposure to H_2O_2 in the 3D model resulted in evident alterations in nuclear organization, with a reduction in nuclear density, partial loss of spheroid compaction, and a more irregular distribution of cells. Furthermore, a decrease in the intensity of the nuclear signal was observed in some regions a finding compatible with DNA damage and the onset of apoptotic processes induced by oxidative stress, as widely described for neurons subjected to ROS (Fan; Hussien; Brooks, 2010).

In the group treated only with the Spike protein, the spheroids presented relative preservation of the three-dimensional architecture, with nuclear density comparable to or slightly higher than that observed in the H_2O_2 group. The nuclei mostly maintained intact morphology, although with slight heterogeneity in size and fluorescent signal intensity. This pattern suggests that, in the three-dimensional environment, Spike exposure did not induce immediate severe nuclear damage, potentially being associated with an initial adaptive or metabolic response of neuronal cells, as proposed in studies indicating modulatory effects of the viral protein on cell survival pathways (Rhea *et al*., 2021).

In contrast, the non-irradiated Spike + H_2O_2 group presented the most pronounced state of nuclear impairment. A significant reduction in nuclear density was observed, along with loss

of spheroid compaction and dispersed nuclei with less intense fluorescent signals. These characteristics are compatible with the activation of apoptotic pathways associated with mitochondrial dysfunction and severe oxidative damage—a phenomenon frequently observed when multiple cellular insults act synergistically (Fan; Hussien; Brooks, 2010; Pendergrass; Wolf; Poot, 2004).

LED irradiation promoted evident protective effects on nuclear integrity in the 3D model. In the irradiated control group, the nuclear pattern remained similar to the non-irradiated control, confirming the absence of PBM toxicity under the experimental conditions. In the H_2O_2 + LED and Spike + LED groups, an increase in nuclear density, better spheroid compaction, and nuclei with more regular morphology were observed compared to the respective non-irradiated groups, indicating an attenuation of the nuclear damage induced by the insults.

Particularly relevantly, in the irradiated Spike + H_2O_2 group, the application of LED resulted in partial preservation of nuclear organization, with a higher number of intact nuclei and recovery of spheroid compaction. These findings are in line with the literature describing PBM as capable of modulating mitochondrial metabolism, reducing oxidative stress, and limiting the activation of apoptotic pathways, indirectly contributing to the preservation of nuclear integrity (Salehpour *et al*., 2018; Hamblin, 2017).

The comparison between the 2D and 3D models reinforces the higher sensitivity of the three-dimensional system. While in the 2D model Spike exposure predominantly resulted in preserved nuclei, in the 3D model spike + H_2O_2 combination revealed more severe nuclear alterations, evidencing that the three-dimensional architecture, by reproducing metabolic gradients and greater dependence on structural cohesion, more clearly exposes cellular damage mechanisms associated with oxidative stress and mitochondrial dysfunction (Edmondson *et al*., 2014; Ravi *et al*., 2015).

5.4 MITOCHONDRIAL MORPHOLOGY AND FUNCTIONALITY

A The analysis of mitochondrial morphology and functionality, through MitoTracker staining, revealed significant differences among the experimental groups. In the two-dimensional model (Figure 10), the control group exhibited a well-organized pattern, with a diffuse and homogeneous signal in the cytoplasm, distributed in a reticular fashion along the neuronal processes, characteristic of an intact and functional mitochondrial network.

Cells exposed to the Spike protein showed a partial alteration of this pattern, with more punctate mitochondria, network fragmentation, and a reduction in fluorescent intensity in some

cells. Furthermore, a decreased distribution of the staining was observed in the neuronal processes, indicating an impairment of local energy support.

Oxidative stress proved to be a critical factor for mitochondrial integrity. The H_2O_2 treated group exhibited a strong mitochondrial redistribution, with marked network fragmentation and a reduction in the number of functional mitochondria, consistent with a process of excessive mitochondrial fission induced by oxidative stress. This pattern was even more evident in the Spike + H_2O_2 group, in which intense fragmentation, a global reduction in the fluorescent signal, and an almost complete absence of staining in the neuronal processes were observed, indicating a collapse of the mitochondrial network.

On the other hand, the groups treated with PBM (Spike + LED; H_2O_2 + LED; Spike + H_2O_2 + LED) presented partial preservation of mitochondrial morphology. In these groups, the signal appeared more diffuse and reticular compared to the non-irradiated groups under stress, with a greater presence of mitochondria in the neuronal processes.

Figure 10 – Micrographs of mitochondrial staining in differentiated neuronal cells, non-irradiated (top row) and irradiated with PBM (bottom row) in a 2D model under the following conditions: Control, H_2O_2, Spike, and Spike + H_2O_2, stained with MitoTracker. Control cells exhibited an organized and reticular mitochondrial appearance. Cells exposed to the spike protein showed reduced intensity and partial fragmentation. Exposure to H_2O_2 induced severe fragmentation (enlarged yellow area) and mitochondrial loss, while the Spike + H_2O_2 group exhibited pronounced perturbations (enlarged white area). The groups treated with PBM demonstrated visibly improved mitochondrial organization and reduced fragmentation. Scale bars: 10 µm

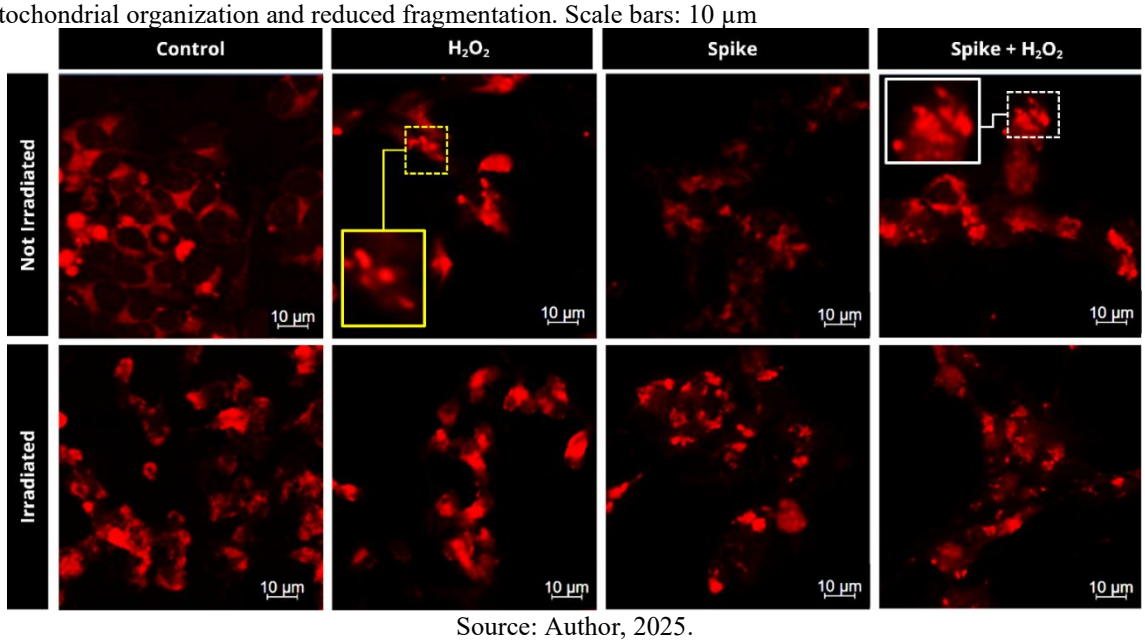

Source: Author, 2025.

The mitochondrial fragmentation observed in the groups exposed to H_2O_2 is in line with the literature, which describes oxidative stress as a potent inducer of mitochondrial fission, loss of membrane potential, and early activation of apoptosis (Fan; Hussien; Brooks, 2010). The reduction of labeling in neuronal processes indicates a deficit in mitochondrial transport and

anchoring processes that are dependent on the integrity of the actin cytoskeleton and microtubules.

In the case of the spike protein, the partial alteration of mitochondrial morphology may be related to its interaction with cell adhesion pathways and cytoskeleton reorganization. Evidence indicates that the aberrant activation of the FAK pathway and the resulting redox imbalance from this interaction can overload mitochondrial function, favoring fragmentation processes (Simons *et al*., 2021).

The intensification of mitochondrial damage in the Spike + H_2O_2 group reinforces the hypothesis of a synergistic effect between the viral protein and oxidative stress. The almost complete loss of the mitochondrial network and its distribution in the processes suggests the activation of the intrinsic apoptotic pathway, in which mitochondrial dysfunction precedes the release of cytochrome C and caspase activation (Pendergrass; Wolf; Poot, 2004).

The partial preservation observed in the LED treated groups can be explained by the action of PBM on CCO, promoting improved ATP production, stabilization of the mitochondrial membrane potential, and modulation of the redox balance (Salehpour *et al*., 2018). These mechanisms justify the partial maintenance of mitochondrial morphology even under conditions of severe stress.

The analysis of mitochondrial morphology and distribution in the three-dimensional model revealed striking alterations in the organization of the mitochondrial network in response to Spike protein exposure, H_2O_2 induced oxidative stress, and PBM (Figure 11). In the non-irradiated control group, a diffuse and homogeneous mitochondrial pattern was observed, with the signal distributed relatively continuously throughout the spheroid. The mitochondria were predominantly organized, forming a network compatible with metabolically active and structurally intact cells. This pattern is characteristic of viable 3D systems, in which mitochondrial dynamics are essential to sustain energy metabolism and cell survival in environments with oxygen and nutrient gradients (Edmondson *et al*., 2014; Ravi *et al*., 2015).

Figure 11 - Micrographs of mitochondrial staining in differentiated neuronal cells, non-irradiated (top row) and irradiated with PBM (bottom row) in a 3D model under the following conditions: Control, H_2O_2, Spike, and Spike + H_2O_2. In the control group, an organized and intense mitochondrial network is observed, with a reticular distribution characteristic of viable models. In the group exposed only to the spike protein, a slight reduction in signal intensity and early signs of network fragmentation are noted. Exposure to peroxide resulted in severe impairment, evidenced by a punctate mitochondrial pattern and loss of the network's structural integrity. The Spike + H_2O_2 group presented the most critical state of disorganization, with dispersed fluorescent signal and fragmentation, indicating severe bioenergetic failure. In contrast, the irradiated groups (bottom row) demonstrated mitochondrial organization with visible improvement and reduced fragmentation compared to their stressed counterparts, suggesting that PBM assisted in preserving mitochondrial function and attenuating the damage induced by the insults. Scale bars: 10 µm.

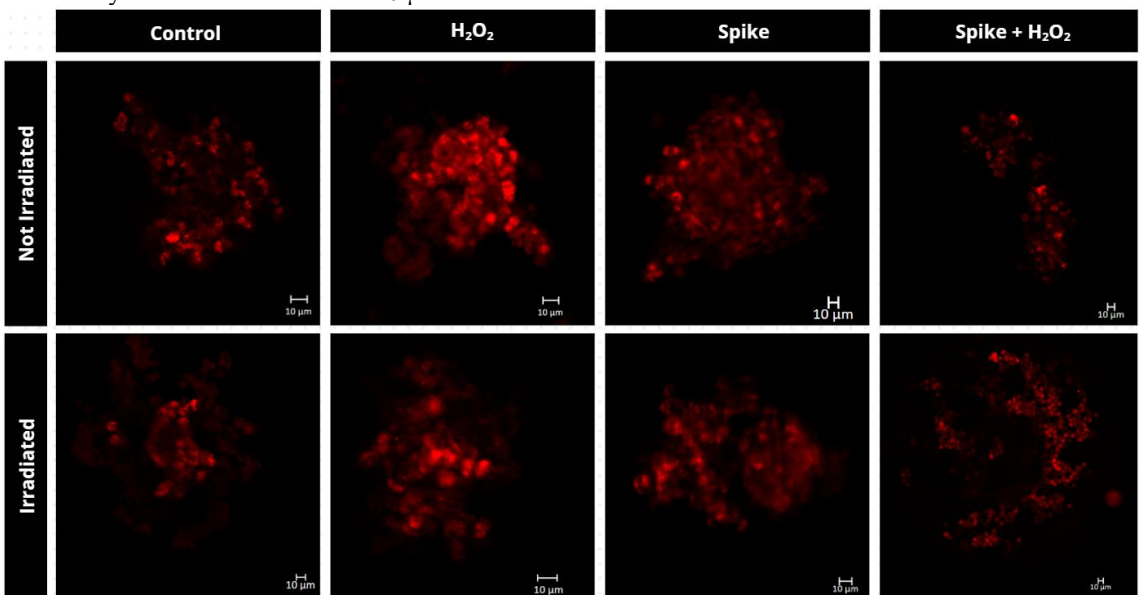

Source: Author, 2025.

Exposure to H_2O_2 promoted evident alterations in mitochondrial morphology, characterized by an increase in the punctate intensity of the fluorescent signal, network fragmentation, and loss of the homogeneous distribution observed in the control. This pattern is compatible with excessive mitochondrial fission induced by oxidative stress, a phenomenon widely described as an early event in the activation of the intrinsic apoptotic pathway (Fan; Hussien; Brooks, 2010; Youle; Van der Bliek, 2012). In the three-dimensional context, such alterations suggest impairment of the mitochondrial membrane potential and a reduction in the metabolic efficiency of cells located in both the periphery and the innermost regions of the spheroid.

In the group treated only with the spike protein, an intermediate mitochondrial pattern was observed. Although the overall architecture of the spheroid was partially preserved, mitochondrial labeling showed areas of higher intensity and the onset of network fragmentation, especially in peripheral regions. This finding suggests that Spike is capable of modulating mitochondrial dynamics even in the absence of a classic oxidative stressor, possibly through the indirect activation of cellular stress pathways and redox imbalance, as described in studies

associating the viral protein with mitochondrial dysfunction and altered neuronal energy metabolism (Singh *et al*., 2020; Rhea *et al*., 2021).

The combination of Spike + H_2O_2 resulted in the most severe case of mitochondrial impairment. A sharp loss of network organization was observed, with a predominance of highly fragmented signals and a reduction in mitochondrial connectivity throughout the spheroid. In some regions, labeling appeared concentrated in intensely fluorescent punctate structures, indicative of dysfunctional mitochondria. This pattern suggests a collapse of mitochondrial dynamics, compatible with loss of membrane potential, accumulation of reactive oxygen species, and activation of cell death pathways (Pendergrass; Wolf; Poot, 2004; Fan; Hussien; Brooks, 2010). These findings reinforce the hypothesis of a synergistic effect between the spike protein and oxidative stress on cellular energy impairment.

PBM by LED promoted evident protective effects on mitochondrial morphology in the 3D model. In the irradiated control group, the mitochondrial pattern remained similar to that of the non-irradiated control, confirming the absence of deleterious LED effects on mitochondrial function. In the H_2O_2 + LED and Spike + LED groups, greater preservation of the mitochondrial network was observed, with a more diffuse signal and reduced fragmentation compared to the respective non-irradiated groups. These findings indicate that PBM contributed to the partial maintenance of mitochondrial membrane potential and structural organization.

Particularly relevantly, in the irradiated Spike + H_2O_2 group, the application of LED resulted in a significant attenuation of mitochondrial fragmentation. Although the network was not completely restored to the control pattern, greater signal continuity and a lower predominance of punctate mitochondria were observed. This effect is consistent with literature describing PBM as capable of stimulating Cytochrome C Oxidase activity, increasing ATP production, and modulating the redox balance, thereby reducing the progression of mitochondrial dysfunction under stress conditions (Karu, 1999; Salehpour *et al*., 2018; Hamblin, 2017).

The comparison between 2D and 3D models highlights important differences in mitochondrial response. In the 2D model, although mitochondrial fragmentation was also observed after exposure to Spike and H_2O_2, the loss of structural organization was less pronounced than in the three-dimensional system. In the 3D model, the dependence of cells on mitochondrial network integrity to sustain spheroid cohesion makes the effects of mitochondrial dysfunction more evident and biologically relevant (Edmondson *et al*., 2014; Ravi *et al*., 2015). Thus, the three-dimensional model reveals more sensitively the energy collapse induced by the

association between the spike protein and oxidative stress, as well as the partial neuroprotective potential of photobiomodulation.

5.5 EFFECTS OF DA PHOTOBIOMODULATION ON VIABILITY AND STRUCTURAL INTEGRITY

The evaluation of the effects of PBM confirmed both the safety of the treatment and its cytoprotective potential against the experimental challenges (Figure 12). Initially, it was observed that the control groups treated only with LED (in both models) presented no metabolic or morphological alterations compared to the non-irradiated controls. This demonstrates the absence of intrinsic toxicity of the technique under the conditions used for differentiated SH-SY5Y cells, reinforcing the non-invasive nature of PBM.

Although the recovery was not complete enough to reach control levels, clear signs of damage attenuation were observed when compared to the corresponding non-LED groups:

i. Spike + LED: There was a lower frequency of condensed nuclei, partial maintenance of neuronal processes, a more organized redistribution of FAK, and a less fragmented mitochondrial network compared to the group exposed only to the S protein.
ii. H_2O_2 + LED: A higher nuclear density, less neurite retraction, and a less punctate mitochondrial pattern were observed than in the group treated only with H_2O_2.
iii. Spike + H_2O_2 + LED: Even in the face of combined exposure, the remaining cells exhibited a higher number of intact nuclei, more preserved processes, and a less fragmented mitochondrial signal than in the Spike + H_2O_2 group without LED.

Figure 12 – Mitochondrial and nuclear morphology of differentiated neuronal cells exposed to the Spike protein, with or without photobiomodulation (PBM) in a 2D model. Immunofluorescence images of non-irradiated groups (top row) and PBM-irradiated groups (bottom row). Mitochondria were labeled with MitoTracker (red), and nuclei were stained with DAPI (blue). PBM (660 nm, 3 J/cm²) attenuated mitochondrial fragmentation and preserved nuclear morphology in the irradiated Spike group, where mitochondria appear less punctate and nuclei exhibit more uniform chromatin compared to the corresponding non-irradiated Spike panel. Scale bars: 10 µm.

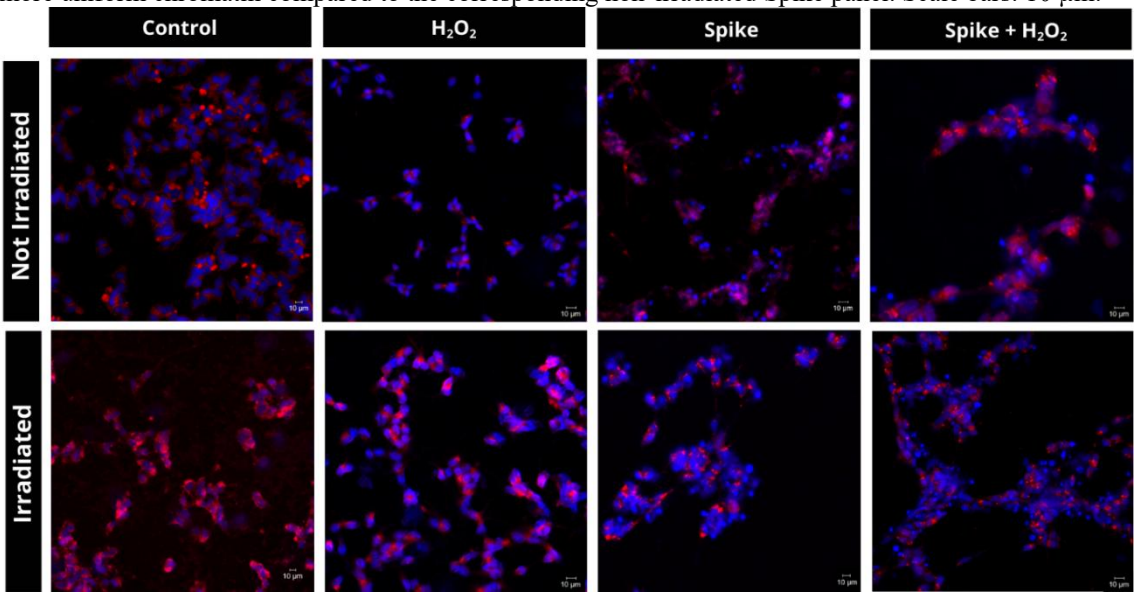

Source: Author, 2025.

These findings find support in the classic mechanism of action of PBM, which involves the absorption of photons by CCO. This interaction optimizes the electron transport chain, increases ATP production, and modulates the redox balance, conferring greater cellular resistance (Karu, 1999; Hamblin, 2016). Furthermore, the literature suggests that PBM activates survival pathways such as PI3K/Akt and ERK, reducing caspase-mediated apoptosis (Fernandes *et al*., 2019). Such processes explain the observed preservation of adhesion and the cytoskeleton, as mitochondrial stability prevents the structural degradation cascade.

The analysis in the 3D model reinforced the 2D findings but revealed important nuances regarding the efficacy of PBM in environments of greater complexity. The spheroids subjected to PBM showed greater preservation of metabolic activity and structural organization. While the H_2O_2 and Spike + H_2O_2 groups without LED exhibited marked disorganization and reduced cell density, the irradiated groups maintained more compact aggregates and mostly intact nuclei.

Regarding mitochondrial dynamics in 3D (Figure 13), PBM contributed to maintaining network continuity, reducing the intense fragmentation associated with energy dysfunction. This effect is in line with studies demonstrating that PBM favors mitochondrial fusion processes, mitigating the damage caused by ROS (Youle; Van Der Bliek, 2012; Hamblin, 2017).

Figure 13 – Mitochondrial and nuclear morphology of differentiated neuronal cells exposed to the Spike protein, with or without photobiomodulation (PBM) in a 3D model. Immunofluorescence images of non-irradiated groups (top row) and PBM-irradiated groups (bottom row). Mitochondria labeled with MitoTracker (red) and nuclei with DAPI (blue). In the control group, high cell density and an organized mitochondrial network are observed. Exposure to H_2O_2 and the Spike protein promoted mitochondrial fragmentation (punctate appearance) and nuclear disorganization, with severe damage in the Spike + H_2O_2 group. PBM (bottom row) visibly attenuated these damages, preserving mitochondrial and nuclear morphology, especially in the Spike group, where more uniform chromatin and integrated mitochondria are observed. Scale bars: 10 µm.

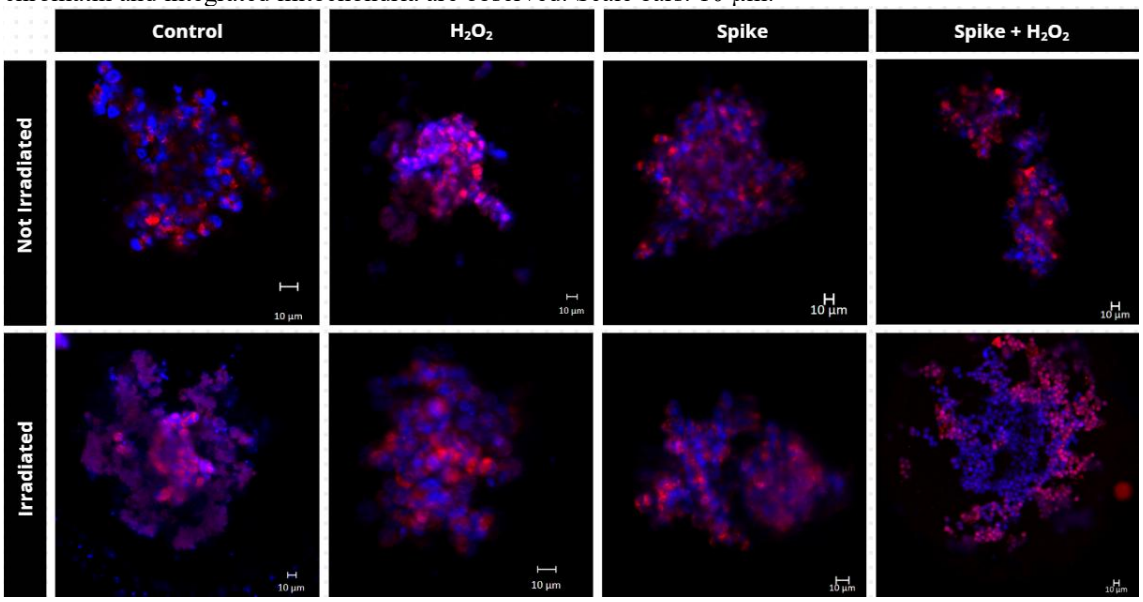

Source: Author, 2025.

However, it was observed that the response in the 3D system was more gradual and heterogeneous. This difference compared to the 2D model can be attributed to the intrinsic characteristics of the three-dimensional architecture, such as diffusion limitations characterized by oxygen and nutrient gradients, as well as the attenuation of the light stimulus itself through the cellular layers. Another characteristic of this model is its biological complexity, involving the influence of cell-cell and cell-extracellular matrix interactions (Edmondson *et al*., 2014; Ravi *et al*., 2015).

In the specific context of the Spike protein, PBM appears to partially attenuate the deleterious effects related to secondary oxidative stress, which have already been described in neuronal models (Rhea *et al*., 2021). The maintenance of structural integrity in the Spike + LED groups suggests that the modulation of mitochondrial metabolism reduces neuronal vulnerability to damage induced by the viral protein, even if it does not completely neutralize it.Taken together, the results from both models consolidate PBM as a promising strategy for preserving cellular homeostasis under conditions of oxidative stress and viral neurotoxicity. The convergence of data between the 2D and 3D systems reinforces the reliability of the

findings, while the particularities of the 3D model offer a more realistic and faithful understanding of the therapeutic application of PBM in neural tissues.

The observed protective effects are in agreement with studies demonstrating that PBM can modulate cell survival pathways, reduce caspase activation, and increase neuronal resistance to oxidative stress (Hamblin, 2016; Salehpour *et al*., 2018). Although recovery was not complete, the data indicate that the LED acts as a modulator capable of attenuating structural and metabolic damage induced by different insults.

5.6 OXIDATIVE STRESS AND CELLULAR IMPAIRMENT

The micrographs revealed striking differences in cellular organization and integrity among the experimental groups, reflecting responses dependent on both the type of stimulus and the architecture of the model used. In the two-dimensional (2D) model, the control group presented intact nuclei, with homogeneous distribution and preserved morphology (Figure 14). In contrast, exposure to hydrogen peroxide resulted in a sharp drop in cell viability, reaching approximately 60% relative to the control (Salles *et al*., 2025). Interestingly, despite this drastic metabolic impairment, the total number of adhered cells did not differ significantly, suggesting that the cells remain fixed to the substrate even in the early stages of degeneration. Morphologically, a notable reduction in cell density and confluence was observed, with twisted and retracted neurites, which reinforces the direct relationship between reactive oxygen species and cytoskeletal instability associated with the reorganization of actin and microtubules (Han *et al*., 2013).

Figure 14 - Evaluation of nuclear and mitochondrial morphology in a 2D model under oxidative stress, using cells differentiated into a neuronal phenotype under non-irradiated (top row) and PBM-irradiated (660 nm, 3 J/cm²; bottom row) conditions. Nuclei were stained with DAPI (blue) and mitochondria with MitoTracker Orange (red). In the control group, preserved cell confluence and a reticular mitochondrial network are observed. Exposure to H_2O_2 resulted in intense neurite retraction, nuclear condensation, and fragmentation of the mitochondrial network. The Spike + H_2O_2 group exhibited the highest degree of structural damage, with a drastic reduction in cell density. In the irradiated groups (bottom row), an attenuation of cytoplasmic retraction and better preservation of nuclear and mitochondrial integrity are noted compared to their respective stressed controls. Scale bar: 10 μm.

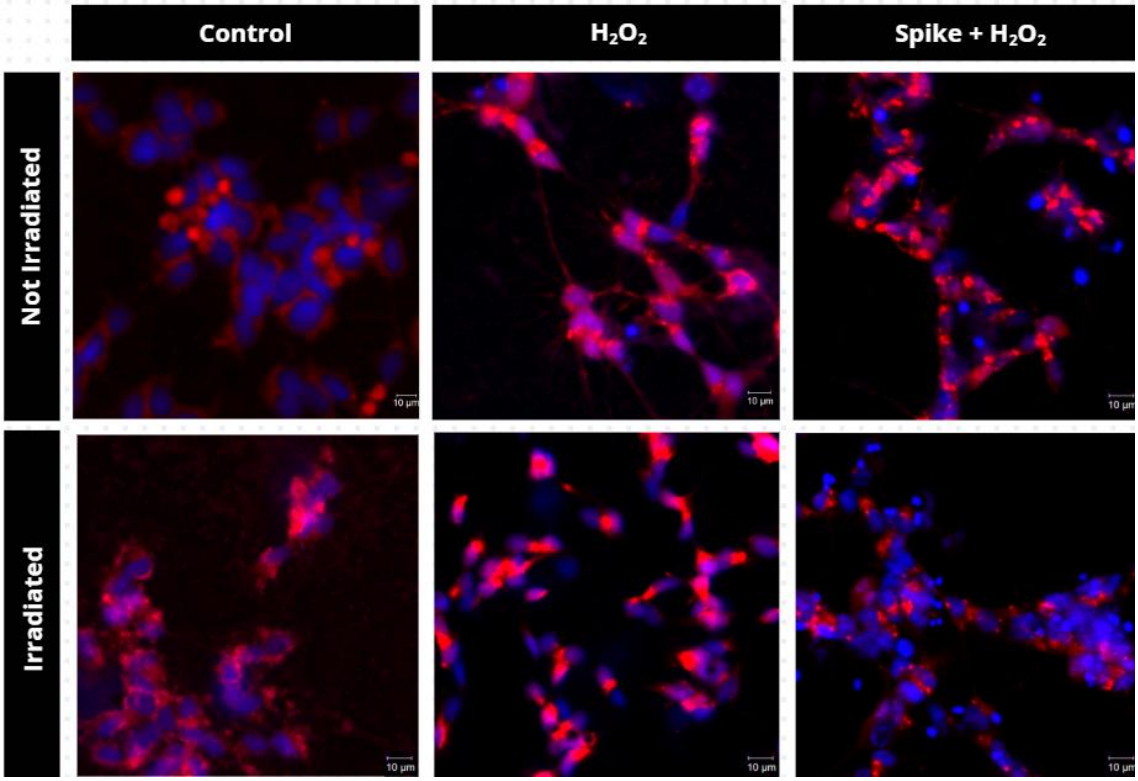

Source: Author, 2025.

The analysis of oxidative stress and cellular impairment in 3D models revealed more modulated responses compared to the 2D system (Figure 15). In the control spheroids, cells exhibited a homogeneous distribution and well-defined nuclei, a characteristic pattern of viable and organized models (Edmondson *et al*., 2014; Ravi *et al*., 2015). Exposure to H_2O_2 in the 3D model promoted nuclear condensation and reduced cellular cohesion, albeit in a less abrupt manner. This behavior is consistent with the literature, which describes the existence of oxygen and nutrient gradients in 3D cultures, capable of attenuating uniform exposure to stress and resulting in greater adaptive capacity (Ravi *et al*., 2015; Edmondson *et al*., 2014).

In the case of the isolated Spike protein, a moderate reduction in the number of nuclei and discrete structural alterations were observed, suggesting that the viral protein may interfere with signaling pathways related to adhesion and survival without necessarily inducing immediate cell death (Rhea *et al*., 2021). However, the association of the spike protein with oxidative stress resulted in the most pronounced state of structural impairment, with spheroid fragmentation and intensely condensed nuclei. This synergistic effect indicates that oxidative

stress acts as an amplifier of the dysfunctions induced by the viral protein, surpassing the basal resistance of the system (Fan, Hussien, and Brooks, 2010; Singh *et al*., 2020).

Figure 15 - Evaluation of nuclear and mitochondrial morphology in a 3D model under oxidative stress, using cells differentiated into a neuronal phenotype under non-irradiated (top row) and PBM-irradiated (660 nm, 3 J/cm^2; bottom row) conditions. Nuclei were stained with DAPI (blue) and mitochondria with MitoTracker Orange (red). In the control group, high cellular compaction and a homogeneous mitochondrial signal are observed. Exposure to H_2O_2 alone promoted the destabilization of the spheroid architecture, with loss of cohesion and punctate mitochondrial fragmentation. In the Spike + H_2O_2 group, the most severe impairment of tissue integrity is observed, with clear disintegration of the spheroidal structure. The application of PBM (bottom row) contributed to maintaining the compaction of cellular aggregates and stabilizing mitochondrial morphology against oxidative and viral insults. Scale bar: 10 µm.

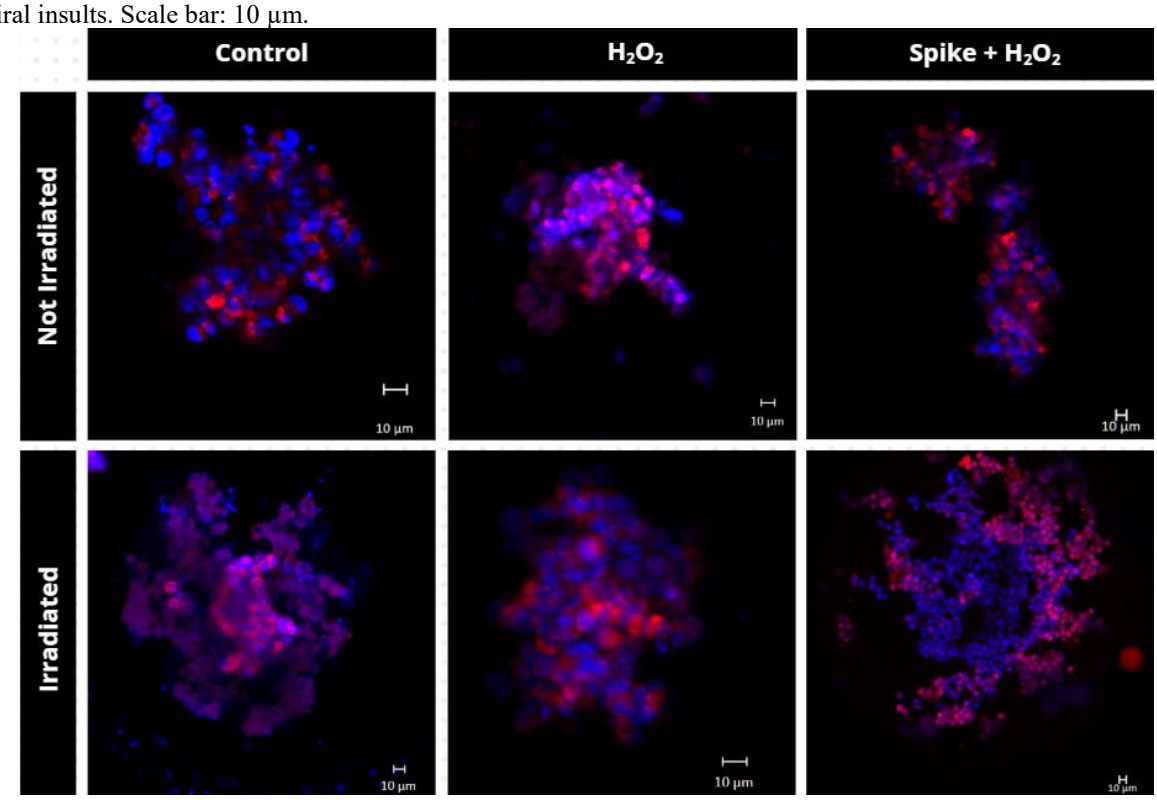

Source: Author, 2025.

The mitochondrial analysis reinforces this interpretation, as the groups subjected to severe oxidative stress exhibited patterns of intense fragmentation. The mitochondrion, being simultaneously a source and a target of ROS, plays a central role in this response; the transition of the mitochondrial network to a punctate pattern is an early marker of apoptosis and bioenergetic dysfunction (Fan; Hussien; Brooks, 2010; Youle; Van Der Bliek, 2012). In this scenario, the application of PBM by LED confirmed both the safety of the technique and its cytoprotective potential. In the irradiated control group, no alterations were observed, demonstrating the absence of intrinsic toxicity. In the groups under stress, the LED promoted a clear attenuation of the damage: there was a lower frequency of condensed nuclei, partial

maintenance of neuronal processes, a more organized redistribution of FAK, and a significantly more preserved mitochondrial network.

The mechanism of action of PBM is widely associated with the absorption of light by Cytochrome C Oxidase, which promotes an increase in enzymatic activity, improves ATP production, and modulates the redox balance (Karu, 1999; Hamblin, 2016; Salehpour *et al*., 2018). In the 3D model, although the protective effects appeared more gradual and heterogeneous due to light and nutrient diffusion limitations, the preservation of nuclear organization and spheroid compaction was evident (Edmondson *et al*., 2014; Ravi *et al.*, 2015). Studies indicate that PBM can induce protective intracellular signaling, such as the PI3K/Akt and ERK pathways, in addition to favoring mitochondrial fusion processes and reducing neuroinflammation (Fernandes et al., 2019; Hamblin, 2017). Taken together, the comparison between the 2D and 3D models reinforces that the three-dimensional architecture more realistically exposes the mechanisms of cellular damage and recovery. These findings consolidate PBM as a strategy capable of partially preserving cell viability and structural integrity, even under adverse conditions of oxidative stress and insults associated with the Spike protein (Salehpour *et al.*, 2020).

5.7 CYTOSKELETON ORGANIZATION AND CELL ADHESION

Exposure of SH-SY5Y cells, differentiated into a neuronal phenotype, to the S protein resulted in significant morphological and cellular alterations, revealing a complex pattern of responses that directly depend on the cellular microenvironment. In the two-dimensional (2D) model, a decrease in cell density was observed, accompanied by a marked intensification in the labeling of Focal Adhesion Kinase (FAK) (Figure 16-B). This finding suggests that, in monolayer culture, the viral protein triggers an initial activation of this pathway as part of a compensatory and adaptive mechanism in response to the aggression (Schlaepfer; Mitra., 2004).

Figure 16 - Cytoskeleton organization, focal adhesion, and nuclear morphology of differentiated neuronal cells exposed or not to the Spike protein in a 2D model. (A) Control condition showing well-organized actin filaments (phalloidin, red), defined focal adhesion sites (FAK, green), and preserved nuclear arrangement (DAPI, blue). The arrows highlight representative structures: actin filaments (red arrow), focal adhesions (green arrow), and preserved nuclear morphology (blue arrow). (B) Cells exposed to the Spike protein (0.5 µg/mL) exhibited cytoskeleton disorganization, altered FAK distribution, and nuclear condensation. Arrows indicate disorganized actin filaments (red arrow), redistributed focal adhesion points (green arrow), and condensed or irregular nuclei (blue arrow). Scale bars: 20 µm.

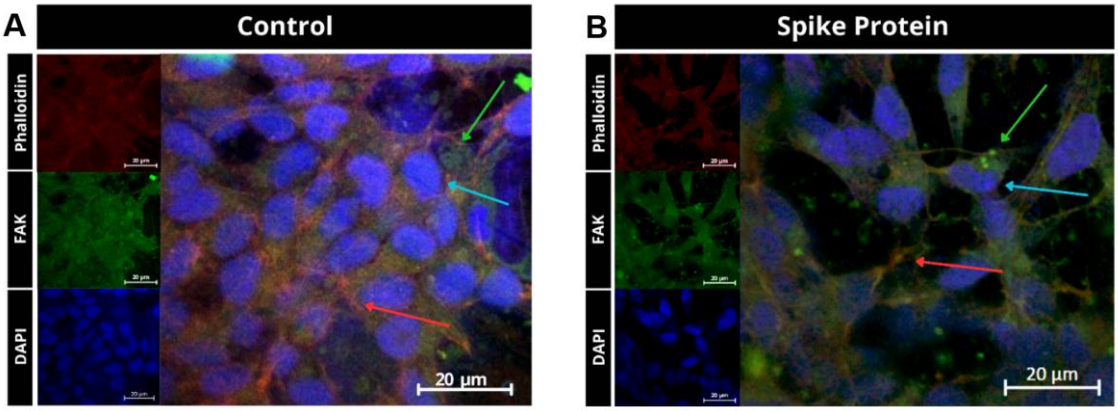

Source: Author, 2025.

However, this scenario contrasts drastically with what was observed in the immunofluorescence analysis of 3D spheroids (Figure 17). While the control group (Figure 17-A) exhibited an organized cytoskeleton, with continuous rhodamine-phalloidin (red) staining and homogeneous distribution of FAK (green) at the periphery, the group treated with the Spike glycoprotein (Figure 17-B) revealed a profound disorganization of the spheroidal architecture. FAK signaling appeared dispersed and with reduced intensity, indicating the impairment of cell-cell and cell-matrix adhesion points and the loss of tissue cohesion (Mitra; Hanson; Schlaepfer, 2005).

Figure 17 - Cytoskeleton organization, focal adhesion, and nuclear morphology of differentiated neuronal cells exposed or not to the Spike protein in a 3D model. (A) Control Group: spheroids present an organized architecture, with continuous actin filaments (phalloidin, red), homogeneously distributed FAK labeling (green), and intact nuclei (DAPI, blue), indicating preservation of structural integrity and tissue cohesion. (B) Exposed Group: exposure to the Spike protein (0.5 µg/mL) resulted in significant disorganization of the three-dimensional architecture. Fragmentation of actin filaments, dispersed redistribution of FAK, and nuclei with irregular or condensed morphology are observed, suggesting impairment of adhesion sites and the structural stability of the spheroid. Scale bars: 20 µm.

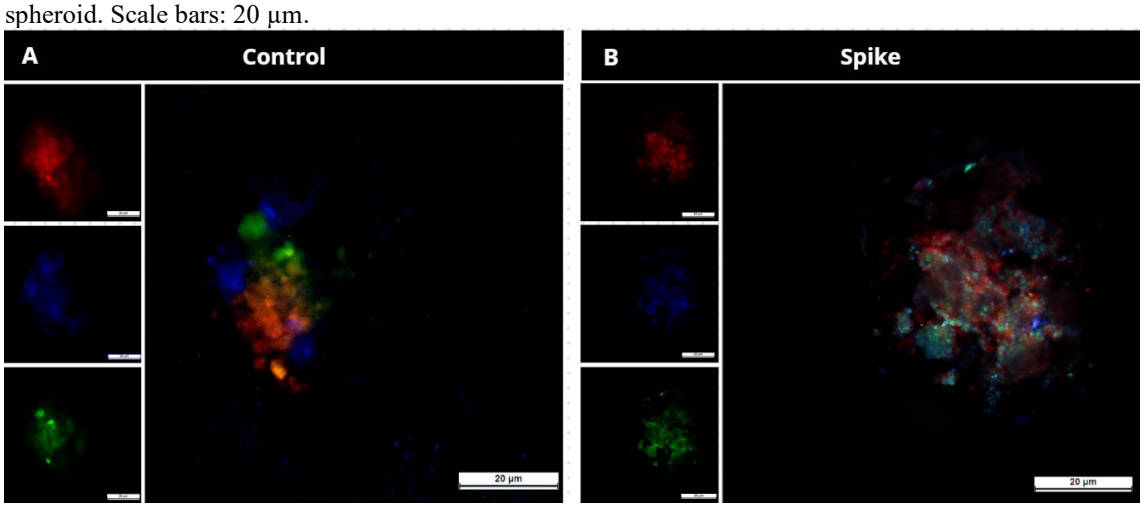

Source: Author, 2025.

In parallel, the disorganization of the actin cytoskeleton was a constant finding, in which phalloidin staining in 3D appeared fragmented and diffuse, reflecting the structural collapse already observed in the 2D model (Figure 16). This effect aligns with literature demonstrating the interaction of the spike protein with receptors such as ACE2 and neuropilin-1, activating intracellular pathways that promote the depolymerization of actin filaments (Dali *et al*., 2020; Cantuti-Castelvetri *et al*., 2020). One of the most notable contrasts lies in the nuclear morphology: while the 2D model maintained preserved nuclei, suggesting interference in stress pathways without immediate cell death (Rhea *et al*., 2021), the 3D model revealed nuclei (DAPI) with irregular and disorganized morphology, classic markers of severe nuclear damage (Kroemer *et al*., 2009).

A controversial and extremely relevant point was observed in the correlation between morphology and cell viability in the 3D model. Despite the evident physical deconstruction, Alamar Blue assays indicated an increase in metabolic viability. This event can be interpreted as a transient compensatory response mediated by the activation of pro-survival pathways and phenotypic reprogramming (Zhang; Yang; Qiang, 2018). However, it must be considered that assays based on redox activity can suffer interference under stress conditions. The increase in ROS production and exacerbated metabolism as an attempt to compensate for cellular damage

can artificially elevate the detected viability index, even in the face of critical structural disorganization (Erikstein *et al*., 2010).

In summary, the integrated morphological data sustain that the S protein modulates neuronal structure in a multiphasic and contextual manner. While the 2D model suggests an initial phase of adaptive activation (via FAK), the 3D model reveals the final systemic collapse: a disorganization that compromises the cytoskeleton, deconstructs adhesion points, and induces nuclear damage (Song *et al*., 2021). The discrepancy between morphological integrity and the metabolic increase reinforces the need for caution in interpreting isolated viability assays and highlights the 3D spheroid model as a superior system for capturing the real toxicity of the viral protein in neural tissues.

6 CONCLUSION

Studies have comprehensively demonstrated that the SARS-CoV-2 S protein induces significant structural and functional alterations in in vitro neuronal models, mimicking key aspects of neurodegenerative processes. Exposure to the viral protein resulted in reduced cell viability, cytoskeleton disorganization, mitochondrial fragmentation, and alterations in focal adhesion signaling mediated by FAK. The combination of the S protein with H_2O_2-induced oxidative stress potentiated these damages, revealing a synergistic mechanism of neurotoxicity in which oxidative stress acts as an amplifier of the dysfunctions induced by the viral protein.

Parallel to this, PBM with LED (660 nm) proved to be a safe intervention with significant neuroprotective potential. PBM partially attenuated the cellular damage induced by both Spike and H_2O_2, demonstrating positive effects on the preservation of mitochondrial integrity, nuclear morphology, and cytoskeletal organization. This therapeutic role is sustained by the LED's ability to modulate mitochondrial metabolism, stabilize the redox balance, and normalize cellular metabolic homeostasis in the face of experimental insults.

The standardization and validation of the 3D spheroid model of SH-SY5Y cells constitute a fundamental methodological advancement of this work. By reproducing metabolic gradients and cell-cell interactions, the three-dimensional system revealed nuances of neuropathogenesis that remain masked in 2D cultures, such as the paradox between increased compensatory metabolic activity and the progressive structural collapse of the spheroid. In the 3D environment, the increased sensitivity of the system more clearly exposed the impairment of cell adhesion and the loss of tissue cohesion resulting from viral exposure.

Finally, the obtained results not only elucidate the neurotoxicity mechanisms of the S protein but also position PBM as an innovative and non-pharmacological strategy for the modulation of neurodegenerative processes. The 3D spheroid model emerges as a critical physiological platform, offering translational perspectives for the development of new therapeutic approaches aimed at Alzheimer's disease and neurological conditions associated with COVID-19.

REFERENCES

BIEDLER, J. L. *et al*. Multiple neurotransmitter synthesis by human neuroblastoma cell lines and clones. **Cancer research**, v. 38, n. 11 Pt 1, p. 3751–3757, 1978.

BIORENDER Team. **Pathology of Alzheimer's Disease**. BioRender Scientific Illustration Platform. 2025. Available at: https://app.biorender.com.

BUTTERFIELD, D. Allan; HALLIWELL, Barry. Oxidative stress, dysfunctional glucose metabolism and Alzheimer disease. Nature reviews. **Neuroscience**, v. 20, n. 3, p. 148–160, 2019.

BUZHDYGAN, Tetyana P. *et al*. The SARS-CoV-2 spike protein alters barrier function in 2D static and 3D microfluidic in-vitro models of the human blood-brain barrier. **Neurobiology of Disease**, v. 146, n. 105131, p. 105131, 2020.

CALABRESE, E. J.; MATTSON, M. P. How does hormesis impact biology, toxicology, and medicine? **NPJ Aging and Mechanisms of Disease,** v. 3, n. 13, p. 1-8, 2017.

CANTUTI-CASTELVETRI, L. et al. Neuropilin-1 facilitates SARS-CoV-2 cell entry and infectivity. **Science** (New York, N.Y.), v. 370, n. 6518, p. 856–860, 2020.

CELL SIGNALING TECHNOLOGY. MitoTracker® Red CMXRos. Disponível em: https://www.cellsignal.com/products/fluorescent-dyes/mitotracker-red-cmxros/9082. Acesso em: 24 set. 2025.

CHEIGNON, C. *et al*. Oxidative stress and the amyloid beta peptide in Alzheimer's disease. **Redox biology**, v. 14, p. 450–464, 2018.

CLOUGH, Erin *et al*. Mitochondrial dynamics in SARS-COV2 spike protein treated human microglia: Implications for neuro-COVID. **Journal of Neuroimmune Pharmacology: The Official Journal of the Society on NeuroImmune Pharmacology**, v. 16, n. 4, p. 770–784, 2021.

CODO, A. C. *et al.* Elevated glucose levels favor SARS-CoV-2 infection and monocyte response through a HIF-1α/glycolysis-dependent axis. Cell Metabolism, v. 32, n. 3, p. 437–446, 2020.

COSTA, Elisabete C. *et al*. 3D tumor spheroids: an overview on the tools and techniques used for their analysis. **Biotechnology advances**, v. 34, n. 8, p. 1427–1441, 2016.

DALY, James L. *et al*. Neuropilin-1 is a host factor for SARS-CoV-2 infection. **Science** (New York, N.Y.), v. 370, n. 6518, p. 861–865, 2020.

EDMONDSON, R. *et al*. Three-dimensional cell culture systems and their applications in drug discovery and cell-based biosensors. **Assay and Drug Development Technologies**, v. 12, n. 4, p. 207–218, 2014.

ERIKSTEIN, Bjarte S. *et al*. Cellular stress induced by resazurin leads to autophagy and cell death via production of reactive oxygen species and mitochondrial impairment. **Journal of Cellular Biochemistry**, v. 111, n. 3, p. 574–584, 2010.

EVANGELISTI, Elisa *et al*. Plasma membrane injury depends on bilayer lipid composition in Alzheimer's disease. **Journal of Alzheimer's disease: JAD**, v. 41, n. 1, p. 289–300, 2014.

FALCO, Anna De *et al*. Doença de Alzheimer: hipóteses etiológicas e perspectivas de tratamento. **Quimica nova**, v. 39, n. 1, p. 63-80, 2016.

FAN, Xiying; HUSSIEN, Rajaa; BROOKS, George A. H_2O_2-induced mitochondrial fragmentation in C2C12 myocytes. **Free radical biology & medicine**, v. 49, n. 11, p. 1646–1654, 2010.

FELES, Sebastian *et al*. Streamlining culture conditions for the neuroblastoma cell line SH-SY5Y: A prerequisite for functional studies. **Methods and protocols**, v. 5, n. 4, p. 58, 2022.

FERNANDES, K. *et al.* Photobiomodulation induces neuroprotective effects through modulation of PI3K/Akt and MAPK/ERK pathways. **Journal of Photochemistry and Photobiology B: Biology**, v. 199, 2019.

FINAUD, J.; LAC, G.; FILAIRE, E. Oxidative stress: relationship with exercise and training. **Sports Medicine**, v. 36, n. 4, p. 327–358, 2006.

FISH, Paul V. *et al*. New approaches for the treatment of Alzheimer's disease. **Bioorganic & medicinal chemistry letters**, v. 29, n. 2, p. 125–133, 2019.

FONTES-DANTAS, Fabricia L. *et al*. SARS-CoV-2 Spike protein induces TLR4-mediated long-term cognitive dysfunction recapitulating post-COVID-19 syndrome in mice. Cell Reports, v. 42, n. 3, p. 112189, 2023.

FREITAS, Lucas Freitas; HAMBLIN, Michael R. Proposed mechanisms of photobiomodulation or low-level light therapy. **IEEE journal of selected topics in quantum electronics**, v. 22, n. 3, p. 348–364, 2016.

GRILLO, S. L. Red and near-infrared photobiomodulation improve cognition and reduce amyloid burden in Alzheimer's disease models. **Brain Research Bulletin**, v. 199, p. 38–47, 2023.

HAMBLIN, Michael R. Shining light on the head: Photobiomodulation for brain disorders. **BBA clinical**, v. 6, p. 113–124, 2016.

HAMBLIN, Michael R. Mechanisms and applications of the anti-inflammatory effects of photobiomodulation. **AIMS biophysics**, v. 4, n. 3, p. 337–361, 2017.

HAMBLIN, Michael R. Photobiomodulation for Alzheimer's disease: Has the light dawned? **Photonics**, v. 6, n. 3, p. 77, 2019.

HAN, Hai-Yan *et al*. αv and β1 Integrins mediate Aβ-induced neurotoxicity in hippocampal neurons via the FAK signaling pathway. **PloS one**, v. 8, n. 6, p. e64839, 2013.

KAPAŁCZYŃSKA, Marta *et al*. 2D and 3D cell cultures – a comparison of different types of cancer cell cultures. **Archives of medical science: AMS**, v. 14, n. 4, p. 910-919, 2018.

KARU, T. Primary and secondary mechanisms of action of visible to near-IR radiation on cells. Journal of photochemistry and photobiology. **B, Biology**, v. 49, n. 1, p. 1–17, 1999.

KHAN, S. *et al*. SARS-CoV-2 spike protein induces inflammation via TLR2-dependent activation of the NF-κB pathway. **Elife**, v. 10, 2021.

KROEMER, G. *et al.* Classification of cell death: recommendations of the Nomenclature Committee on Cell Death 2009. **Cell Death and Differentiation**, v. 16, n. 1, p. 3–11, 2009.

KRUSE R. L. Therapeutic strategies in an outbreak scenario to treat the novel coronavirus originating in Wuhan, China. **F1000Research**, v. 9, n. 72; 2020. https://doi.org/10.12688/f1000research.22211.2

LANCASTER, Madeline A.; KNOBLICH, Juergen A. Generation of cerebral organoids from human pluripotent stem cells. **Nature protocols**, v. 9, n. 10, p. 2329–2340, 2014.

LANGHANS, Sigrid A. Three-dimensional in vitro cell culture models in drug discovery and drug repositioning. **Frontiers in pharmacology**, v. 9, p. 6, 2018.

LUSHCHAK, Volodymyr I. Free radicals, reactive oxygen species, oxidative stress and its classification. **Chemico-biological interactions**, v. 224, p. 164–175, 2014.

LYRA, P. R. N. *et al*. In silico evidence of the interaction between the SARS-CoV-2 spike protein and the prion protein. **Journal of Toxicology and Environmental Health, Part A**, v. 85, n. 5, p. 201–209, 2022.

MITRA, Satyajit K.; HANSON, Daniel A.; SCHLAEPFER, David D. Focal adhesion kinase: in command and control of cell motility. **Nature Reviews. Molecular Cell Biology**, v. 6, n. 1, p. 56–68, 2005.

OH, J. M. *et al.* SARS-CoV-2 Spike Protein Induces Neuroinflammation via TLR2 Activation**. International Journal of Molecular Sciences**, v. 23, n. 21, 2022.

OLAJIDE, O. A. *et al*. SARS-CoV-2 Spike Glycoprotein S1 Induces Neuroinflammation in BV-2 Microglia. **Molecular Neurobiology**, v. 59, n. 1, p. 445–458, 2022. DOI: https://doi.org/10.1007/s12035-021-02593-6.

PARK, Joseph *et al*. A 3D human triculture system modeling neurodegeneration and neuroinflammation in Alzheimer's disease. **Nature neuroscience**, v. 21, n. 7, p. 941–951, 2018.

PENDERGRASS, W.; WOLF, N.; POOT, M. Efficacy of MitoTracker Green and CMXrosamine to measure changes in mitochondrial membrane potentials in living cells and tissues. **Cytometry. Part A: the journal of the International Society for Analytical Cytology**, v. 61, n. 2, p. 162–169, 2004.

PURUSHOTHUMAN, Sivaraman *et al*. Photobiomodulation with near infrared light mitigates Alzheimer's disease-related pathology in cerebral cortex - evidence from two transgenic mouse models. *Alzheimer's research & therapy*, v. 6, n. 1, p. 2, 2014.

RAVI, Maddaly *et al*. 3D cell culture systems: advantages and applications: 3D cell culture systems. **Journal of Cellular Physiology**, v. 230, n. 1, p. 16–26, 2015.

RHEA, Elizabeth M. *et al*. The S1 protein of SARS-CoV-2 crosses the blood-brain barrier in mice. **Nature neuroscience**, v. 24, n. 3, p. 368–378, 2021.

ROSSATO, Rafaella Carvalho *et al*. Photobiomodulation by LED 660 nm and Taurine against H_2O_2 oxidative stress in SH-SY5Y cells. **Lasers in medical science**, v. 40, n. 1, p. 211, 2025.

SALAMEH, Therese S. *et al*. Central nervous system delivery of intranasal insulin: Mechanisms of uptake and effects on cognition. **Journal of Alzheimer's disease: JAD**, v. 47, n. 3, p. 715–728, 2015.

SALEHPOUR, F. Photobiomodulation therapy: molecular and cellular mechanisms. **Journal of Cellular and Molecular Medicine**, n. 6, p. 2688–2700, 2018.

SALEHPOUR, Farzad *et al*. Brain photobiomodulation therapy: A narrative review. **Molecular neurobiology**, v. 55, n. 8, p. 6601–6636, 2018.

SALEHPOUR, Farzad *et al*. Therapeutic potential of intranasal photobiomodulation therapy for neurological and neuropsychiatric disorders: a narrative review. **Reviews in the Neurosciences**, v. 31, n. 3, p. 269–286, 2020.

SALLES, Geisa R. *et al*. 2D and 3D models of Alzheimer's disease: Investigating neuron-like cells in oxidative environments. **ACS omega**, v. 10, n. 25, p. 27501–27514, 2025.

SCHLAEPFER, David D.; MITRA, Satyajit K. Multiple connections link FAK to cell motility and invasion. **Current Opinion in Genetics & Development**, v. 14, n. 1, p. 92–101, 2004.

SIES, Helmut; JONES, Dean P. Reactive oxygen species (ROS) as pleiotropic physiological signalling agents. Nature reviews. **Molecular cell biology**, v. 21, n. 7, p. 363–383, 2020.

SIMONS, Peter *et al*. Integrin activation is an essential component of SARS-CoV-2 infection. **Scientific reports**, v. 11, n. 1, p. 20398, 2021.

SINGH, Keshav K. *et al*. Decoding SARS-CoV-2 hijacking of host mitochondria in COVID-19 pathogenesis. American Journal of Physiology. **Cell Physiology**, v. 319, n. 2, p. C258–C267, 2020.

SOHEILIFAR, Sepideh; FATHI, Homa; NAGHDI, Navid. Photobiomodulation therapy as a high potential treatment modality for COVID-19. **Lasers in Medical Science**, v. 36, n. 5, p. 935–938, 2021.

SONG, E. *et al*. Neuroinvasion of SARS-CoV-2 in human and mouse brain. **Journal of Experimental Medicine**, v. 218, n. 3, e20202135, 2021. doi: 10.1084/jem.20202135.

STROOPER, Bart; KARRAN, Eric. The cellular phase of Alzheimer's disease. **Cell**, v. 164, n. 4, p. 603–615, 2016.

SWERDLOW, Russell H. Mitochondria and mitochondrial cascades in Alzheimer's disease. **Journal of Alzheimer's disease: JAD**, v. 62, n. 3, p. 1403–1416, 2018.

TEDFORD, Clark E. *et al*. Quantitative analysis of transcranial and intraparenchymal light penetration in human cadaver brain tissue: TRANSCRANIAL AND INTRAPARENCHYMAL LIGHT PENETRATION. **Lasers in surgery and medicine**, v. 47, n. 4, p. 312–322, 2015.

WRAPP, Daniel *et al*. Cryo-EM structure of the 2019-nCoV spike in the prefusion conformation. **Science**, v. 367, n. 6483, p. 1260–1263, 2020.

XICOY, Helena; WIERINGA, Bé; MARTENS, Gerard J. M. The SH-SY5Y cell line in Parkinson's disease research: a systematic review. **Molecular neurodegeneration**, v. 12, n. 1, p. 10, 2017.

YANG, L. *et al.* Photobiomodulation attenuates neurotoxic polarization of macrophages by inhibiting the Not1-Nur77 pathway. **Lasers in Medical Science**, v. 35, n. 2, p. 453–463, 2020a.

YANG, Luodan *et al*. Mitochondria as a target for neuroprotection: role of methylene blue and photobiomodulation. **Translational neurodegeneration**, v. 9, n. 1, p. 19, 2020b.

YOULE, Richard J.; VAN DER BLIEK, Alexander M. Mitochondrial fission, fusion, and stress. **Science** (New York, N.Y.), v. 337, n. 6098, p. 1062–1065, 2012.

ZHANG, J.; YANG; QIANG. Metabolic reprogramming and cancer progression. **Signal Transduction and Targeted Therapy**, p. 1–12, 2018.

ZHANG, N.; CHAI, S.; WANG, J. Assessing and projecting the global impacts of Alzheimer's disease. **Frontiers in Public Health**, v. 12, 2025. DOI: 10.3389/fpubh.2024.1453489

ZHAO, Yan; ZHAO, Baolu. Oxidative stress and the pathogenesis of Alzheimer's disease. **Oxidative medicine and cellular longevity**, v. 2013, p. 316523, 2013.

ANNEX A – CERTIFICATE OF ANALYSIS OF THE SPIKE PROTEIN

LECC
Laboratório de Engenharia de Cultivos Celulares

Certificado de Análise

Produto: Proteína S recombinante de SARS-COV-2
(conforme Wrapp et al., Science, doi: 10.1126/science.abb2507, 2020)

Código: LECC-COV2-AC001

Lote: O-151021

Tampão: PBS, Biotina 50 mM, NaN_3 3 mM, pH 7,4

Linhagem produtora: HEK 293 cultivada em meio quimicamente definido

Forma de apresentação: Líquida

Aparência: Líquido transparente

Concentração (por Nanodrop): 0,25 mg/mL

Purificação: Cromatografia de afinidade

Transporte e armazenamento:
Transportar a 4ºC e armazenar a -20ºC ou -80ºC. O armazenamento a -20ºC já demonstrou garantir a estabilidade da proteína (avaliada por concentração proteica, SDS-PAGE e *Western blot*) por pelo menos 1 ano. Estudos mais longos de estabilidade estão em curso. Após descongelado, sugere-se aliquotar e recongelar para evitar ciclos repetidos de congelamento/ descongelamento.

Concentração usual para ELISA: 3-4 µg/mL (usando 50 µL/poço, ou seja, 150-200 ng/poço)

Testes: SDS-PAGE e *Western blot*

1: Marcador de massa molecular: Precision Plus Protein™ Dual Color (BioRad) 3 uL
2: O-151021 (2,5 ug)

Figura 1: SDS-PAGE corado com Comassie blue e Western blot revelado com soro de pacientes positivos para COVID-19.

Data: 18/01/2023 **Assinatura:** Túlio Macedo Lima

Laboratório de Engenharia de Cultivos Celulares (LECC) - COPPE – Universidade Federal do Rio de Janeiro (UFRJ)
Av. Pedro Calmon, s/nº, Prédio CETER Anexo ao CT, CEP 21941-596, Rio de Janeiro/RJ, Brasil

ANNEX B – PREPRINT OF THE MANUSCRIPT SUBMITTED TO SPRINGER NATURE

From Neurotoxicity to Neuroprotection: Photobiomodulation against the Effects of the SARS-CoV-2 Spike Protein in an Alzheimer's Disease Model

Erick José Nogueira Andrade
University of Vale do Paraíba / Institute for Research and Development
Luiza de Andrade Giraldi
University of Vale do Paraíba / Institute for Research and Development
Milena Yuki Rosental Sudo
University of Vale do Paraíba / Institute for Research and Development
Lucas de Paula Ramos
Claude Bernard University Lyon 1
Geisa Rodrigues Salles
University of Vale do Paraíba / Institute for Research and Development
Cristina Pacheco-Soares
cpsoares@univap.br

University of Vale do Paraíba / Institute for Research and Development

Research Article

Keywords: Neurotoxicity, Morphology, Oxidative Stress, Neuroprotective

Posted Date: December 12th, 2025

DOI: https://doi.org/10.21203/rs.3.rs-8245044/v1

Additional Declarations: No competing interests reported.

ANNEX C – AWARDS AND RECOGNITIONS

XIII COLAOB
RIO DE JANEIRO - BRAZIL - 26-29TH AUGUST 2025

SLABO

POSTER PRESENTATION CERTIFICATE

We certify that the work

INFLUENCE OF SPIKE PROTEIN ON CELL MORPHOLOGY AND ADHESION IN A NEURONAL MODEL

was presented in poster form by
ERICK JOSÉ NOGUEIRA DE ANDRADE
at the XIII Latin American Congress on Artificial Organs and Biomaterials (COLAOB 2025), in Rio de Janeiro, RJ, Brazil, from August 26 to 29, 2025.

authored by

ERICK JOSÉ NOGUEIRA DE ANDRADE,LUIZA GIRALDI,GEISA NOGUEIRA SALLES,CRISTINA PACHECO SOARES

ROSSANA MARA S. M. THIRÉ, DSC
CHAIR OF THE COLAOB 2025
VICE-PRESIDENT OF SLABO

ANA PAULA ROSIFINI ALVES
PRESIDENT OF THE SLABO

INIC 2025 · XXIX INIC · XXV EPG · XIX INIC Jr. · V ENEXUN · XV INID

Certificamos que o trabalho intitulado "AVALIAÇÃO DOS EFEITOS DA PROTEÍNA SPIKE DO SARS-COV-2 EM CÉLULAS SH-SY5Y DIFERENCIADAS EM MODELO NEURONAL 3D" de autoria de Erick José Nogueira de Andrade, Milena Yuki Rosental Sudo e Cristina Pacheco Soares desenvolvido na instituição Universidade do Vale do Paraíba - Univap foi premiado como 1º lugar na área Engenharias no XXV Encontro Latino Americano de Pós-Graduação (XXV EPG), realizado na Universidade do Vale do Paraíba, nos dias 29, 30 e 31 de outubro de 2025.

Prof. Dr. Alan Prestes
Pró-reitor de Pós-Graduação e Pesquisa da Univap
Coordenador Geral do XXIX INIC

São José dos Campos, 31 de outubro de 2025.

Apoio: CNPq · FAPESP · CAPES
Realização: univap – UNIVERSIDADE DO VALE DO PARAÍBA · FUNDAÇÃO VALEPARAIBANA DE ENSINO